Article

Cell Reports

Fasting-Mimicking Diet Modulates Microbiota and Promotes Intestinal Regeneration to Reduce Inflammatory Bowel Disease Pathology

Graphical Abstract

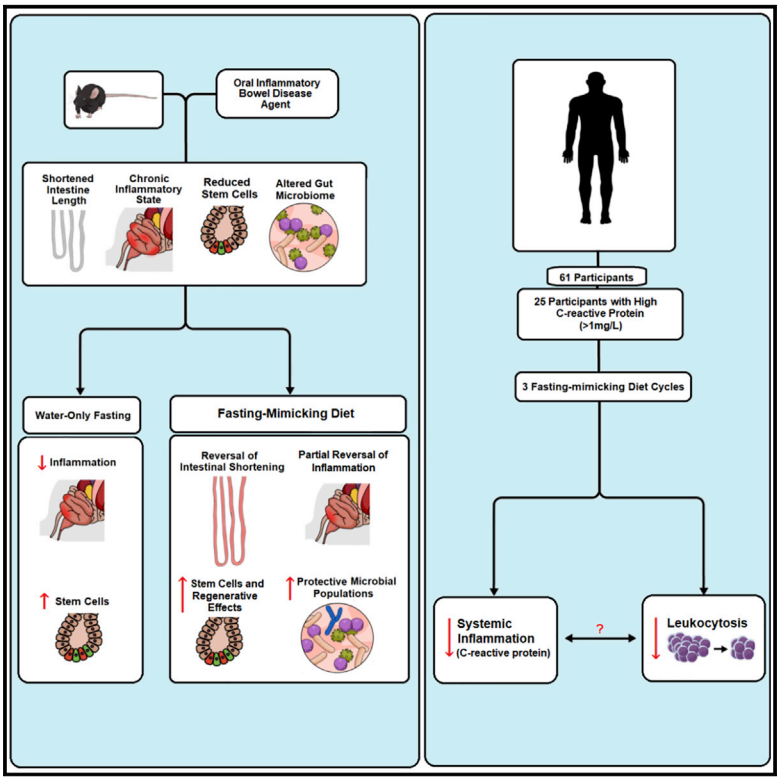

Authors

Priya Rangan, Inyoung Choi, Min Wei, ..., Vanessa Ocon, Maya Abdulridha, Valter D. Longo

Correspondence

vlongo@usc.edu

In Brief

Rangan et al. show that cycles of a fasting-mimicking diet (FMD) ameliorate intestinal inflammation, promote intestinal regeneration, and stimulate the growth of protective gut microbial populations in a mouse model displaying symptoms and pathology associated with IBD. They also show that a similar FMD is safe, feasible, and effective in reducing systemic inflammation and the consequent high levels of immune cells in humans.

Highlights

- FMD cycles partially reverse IBD-related pathology compared to water-only fasting
- FMD cycles reduce intestinal inflammatory and immune and increase regenerative markers
- FMD cycles promote the expansion of *Lactobacillaceae* and *Bifidobacteriaceae*
- FMD cycles can reduce systemic inflammation and consequent leukocytosis in humans

Rangan et al., 2019, Cell Reports *26*, 2704–2719
March 5, 2019
https://doi.org/10.1016/j.celrep.2019.02.019

CellPress

OPEN ACCESS
CellPress

Cell Reports
Article

Fasting-Mimicking Diet Modulates Microbiota and Promotes Intestinal Regeneration to Reduce Inflammatory Bowel Disease Pathology

Priya Rangan,[1,5] Inyoung Choi,[1,5] Min Wei,[1] Gerardo Navarrete,[1] Esra Guen,[1] Sebastian Brandhorst,[1] Nobel Enyati,[2] Gab Pasia,[1] Daral Maesincee,[1] Vanessa Ocon,[1] Maya Abdulridha,[1] and Valter D. Longo[2,3,4,6,*]

[1]Longevity Institute, School of Gerontology, Department of Biological Sciences, University of Southern California, 3715 McClintock Avenue, Los Angeles, CA 90089-0191, USA

[2]USC Dornsife College of Letters, Arts & Sciences, Department of Biological Sciences, University of Southern California, 3551 Trousdale Pkwy, Los Angeles, CA 90089-0191, USA

[3]Eli and Edythe Broad Center for Regenerative Medicine and Stem Cell Research at USC, Keck School of Medicine, University of Southern California, 1425 San Pablo St, Los Angeles, CA 90033, USA

[4]IFOM FIRC Institute of Molecular Oncology, Via Adamello 16, Milano 20139, Italy

[5]These authors contributed equally

[6]Lead Contact

*Correspondence: vlongo@usc.edu

https://doi.org/10.1016/j.celrep.2019.02.019

SUMMARY

Dietary interventions are potentially effective therapies for inflammatory bowel diseases (IBDs). We tested the effect of 4-day fasting-mimicking diet (FMD) cycles on a chronic dextran sodium sulfate (DSS)-induced murine model resulting in symptoms and pathology associated with IBD. These FMD cycles reduced intestinal inflammation, increased stem cell number, stimulated protective gut microbiota, and reversed intestinal pathology caused by DSS, whereas water-only fasting increased regenerative and reduced inflammatory markers without reversing pathology. Transplants of *Lactobacillus* or fecal microbiota from DSS- and FMD-treated mice reversed DSS-induced colon shortening, reduced inflammation, and increased colonic stem cells. In a clinical trial, three FMD cycles reduced markers associated with systemic inflammation. The effect of FMD cycles on microbiota composition, immune cell profile, intestinal stem cell levels and the reversal of pathology associated with IBD in mice, and the anti-inflammatory effects demonstrated in a clinical trial show promise for FMD cycles to ameliorate IBD-associated inflammation in humans.

INTRODUCTION

Inflammatory bowel disease (IBD), which includes Crohn's disease (CD) and ulcerative colitis (UC), is associated with acute and chronic inflammation of the intestine. Risk factors include genetic predisposition and factors that alter gut microbiota, such as antibiotics (Manichanh et al., 2012). Although the effect of nutrition on IBD remains poorly understood, diets that cause pro-inflammatory changes in gut microbiota have consistently been associated with IBD pathogenesis (Kaplan and Ng, 2017).

Periodic fasting (PF) and fasting-mimicking diets (FMDs) have been effective in increasing healthy lifespan or as therapies in mouse models for a variety of diseases (Choi et al., 2017; Lee and Longo, 2016; Brandhorst et al., 2015). FMDs can reduce cancer incidence and aging-associated immunosuppression/immunosenescence, a process aided by hematopoietic stem-cell-based regeneration (Brandhorst et al., 2015; Cheng et al., 2014). Moreover, FMD cycles ameliorate or reverse disease progression in mouse models of multiple sclerosis (MS), and type I, and type II diabetes (Choi et al., 2016; Cheng et al., 2017). Recent studies also showed positive effects of a 24-hour fast on intestinal stem cell function in young and aged mice by a fatty acid oxidation pathway (Mihaylova et al., 2018).

Here, we report on the effect of cycles of a low-calorie and low-protein FMD in the treatment of a mouse model for IBD-related pathology and on its effects on inflammatory markers in humans. Our results indicate that FMD cycles cause a reduction in intestinal inflammation, increase intestinal stem cells (ISCs), and promote the expansion of beneficial gut microbiota, resulting in improvements in IBD-associated phenotypes.

RESULTS

FMD Cycles Ameliorate IBD-Associated Phenotypes

The dextran sodium sulfate (DSS)-induced colitis model is commonly used to study IBD in mice because DSS is a sulfated polysaccharide especially toxic to the colonic epithelium (Dupaul-Chicoine J. et al., 2010; Koblansky et al., 2016). The acute DSS model is implemented over 1–2 weeks and is used to achieve short-term alterations in the intestinal barrier, whereas the chronic DSS mouse model is implemented over a period of 2–4 months to cause long-term effects on intestinal immunity and damage, serving as an effective model for chronic colitis (Wirtz et al., 2017). Because genetic factors for IBD are currently

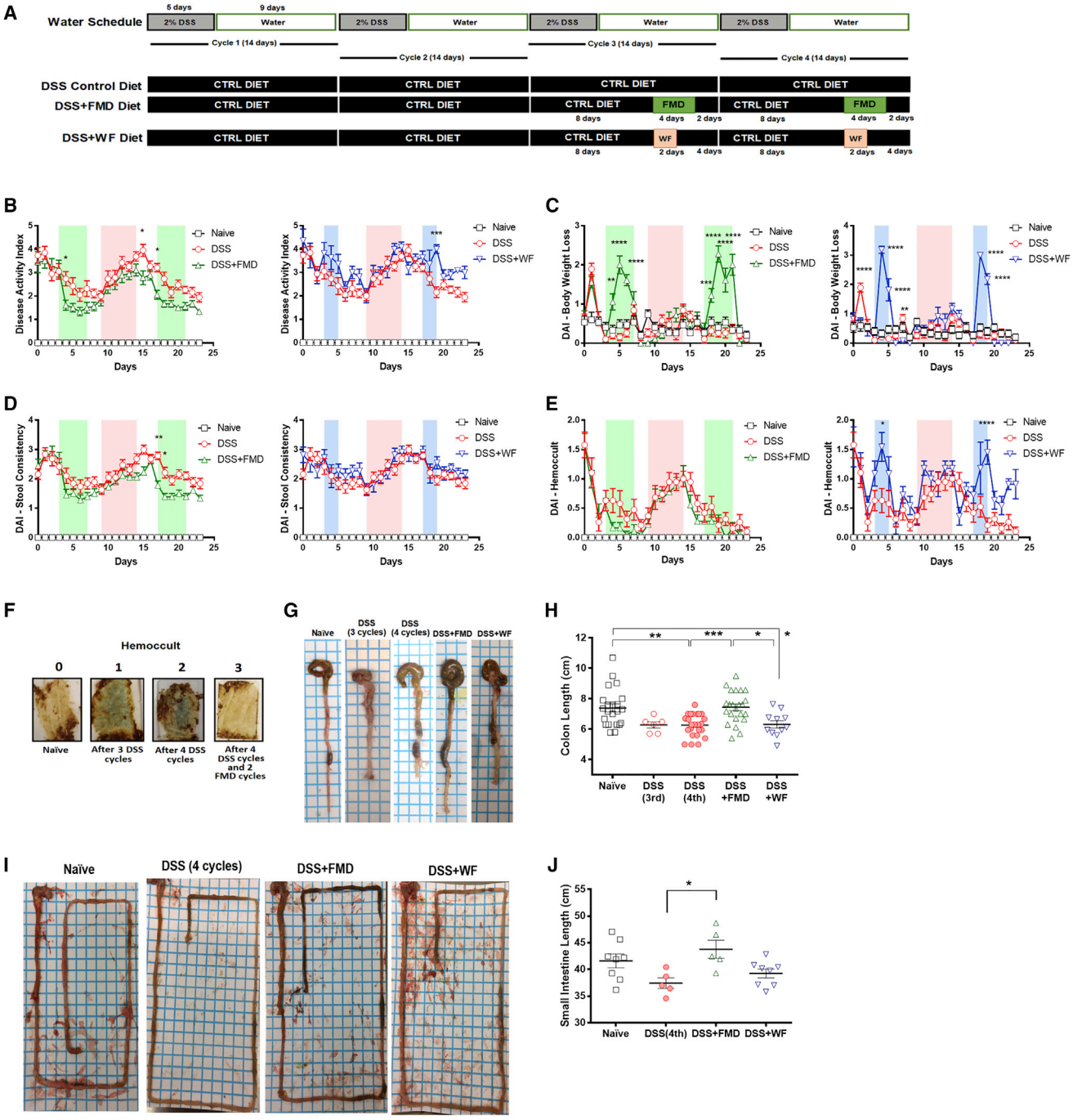

Figure 1. FMD Cycles Ameliorate IBD-Associated Disease Phenotypes and Increase Colon and Small Intestine Lengths

(A) Experimental scheme outlining the water schedule and duration of DSS, DSS+FMD, and DSS+WF diets.

(B) The modified disease activity index (DAI) scores (with body weight loss removed) of the Naive (n = 15), DSS control diet (DSS; n = 19), DSS control diet plus 2 cycles of FMD (DSS+FMD; n = 18), and DSS control diet plus 2 cycles of water-only fasting (DSS+WF; n = 11) groups starting after the third DSS cycle.

(C) The body weight loss variable of the DAI scores of the Naive (n = 15), DSS (n = 19), DSS+FMD (n = 18), and (DSS+WF; n = 11) groups starting after the third DSS cycle.

(D) The stool consistency variable of the DAI scores of the Naive (n = 15), DSS (n = 19), DSS+FMD (n = 18), and DSS+WF (n = 11) groups starting after the third DSS cycle.

(legend continued on next page)

not well-established and only account for a portion of IBD, with one study finding that only 12% of UC patients have a familial history of IBD (Zhang and Li, 2014; Childers et al., 2014), the chronic DSS mouse model is particularly appropriate to model IBDs triggered by environmental factors (Schippers et al., 2016; Hoffmann et al., 2017; Zou et al., 2016).

For our study, we used the chronic DSS mouse model (Chassaing et al., 2014) consisting of 5 days of 2% DSS in the drinking water followed by 9 days of no treatment, which was repeated for a total of 4 cycles (Figure 1A). We evaluated the effects of two, 4-day FMD cycles on symptoms and pathology associated with the disease (Figure 1A), as well as body weight changes and food and water intake during the first three DSS cycles (Figure S1A) and through the two FMD treatments and 4th DSS cycle (Figure S1B). We monitored the following groups: an age-matched, female control that did not receive DSS or FMD (Naive), a disease group administered DSS for 4 cycles together with a standard diet (DSS), and a disease group treated with 4 cycles of DSS in combination with FMD cycles given before and after the 4th DSS treatment (DSS+FMD). During the FMD cycles that flanked the 4th DSS cycle, the DSS+FMD group drank less water because the composition of the FMD contained a substantial amount of water in days 2–4 of the FMD cycle, but during the 4th DSS cycle, water intake of the DSS+FMD group was increased compared to that of the DSS and Naive groups, especially on days 1, 3, and 4 of the 4th DSS cycle (day 1: DSS+FMD versus Naive, $p < 0.001$; day 3: DSS+FMD versus Naive, $p < 0.01$, and DSS+FMD versus DSS, $p < 0.05$; day 4: DSS+FMD versus Naive, $p < 0.01$) (Figure S1B). Thus, the FMD did not negatively affect water intake during the 4th DSS cycle.

Additionally, we studied a group that was treated with 4 cycles of DSS in combination with 2 days of a water-only fast (DSS+WF) before and after the 4th DSS treatment (DSS+WF) (Figure 1A). The DSS+WF group was limited to 2 days per cycle to prevent mice from losing more than 20% of their initial body weight. The same standard is used for the FMDs. Body weight changes and food and water intake were measured everyday through the two water-only fasting treatments preceding and following the 4th and last cycle of DSS treatment (Figure S1C). In the 4th DSS cycle, the water intake of the DSS+WF group was increased, as was seen in the DSS+FMD group, when compared to that of the DSS and Naive groups, especially on days 1, 2, and 4 of the 4th DSS cycle (day 1: DSS+WF versus Naive, $p < 0.001$; day 2: DSS+WF versus Naive, $p < 0.001$, and DSS+WF versus DSS, $p < 0.05$; day 4: DSS+WF versus Naive, $p < 0.05$) (Figure S1C).

Starting on the last day of the 3rd DSS cycle, the disease activity index (DAI) was measured every day for the Naive, DSS, DSS+FMD, and DSS+WF groups. Because an FMD or water-only fast cycle induces a temporary body weight loss, which is not associated with reduced health (Brandhorst et al., 2015) (Figure 1C), our modified DAI scores only include changes in stool consistency and blood in stools (Figures 1D and 1E), as determined by a Hemoccult test (Figure 1F). The DSS+FMD group showed an overall decrease in disease activity when compared to the DSS group starting on day 2 of the first FMD cycle, with significant reductions at the end of the last DSS cycle and at the beginning of the second FMD cycle ($p < 0.05$) (Figure 1B). The DSS+WF group did not display any significant changes in DAI when compared with the DSS group (Figure 1B), except on day 19, which was the 2nd day of the 2nd water-only fast cycle and when the DSS+WF group had a significantly elevated DAI score compared to the DSS group ($p < 0.001$) (Figure 1B). The DSS+WF group also had no significant changes in stool consistency compared to the DSS group (Figure 1D) and was associated with an increase in the presence of blood in stools on day 4 during the 1st water-only fasting cycle ($p < 0.05$) (Figure 1E) and on day 19 during the 2nd water-only fasting cycle ($p < 0.0001$) (Figure 1E) compared to the DSS group, suggesting that in mice, water-only fasting increases gut permeability, at least temporarily.

We also assessed the effects of DSS and the FMD treatment on the white blood cell profile. An increase in the percentage of lymphocytes and decrease in those of granulocytes and neutrophils was observed in mice after 3 cycles of DSS treatment prior to any dietary intervention ($p < 0.001$) (Figures S1D, S1E, and S1G). After 4 DSS cycles, the lymphocyte count, which continued to be elevated compared to that in untreated mice, was reduced by the FMD treatment. The percentages of granulocytes and neutrophils were instead increased in the DSS+ FMD group when compared to the DSS group ($p < 0.05$) (Figures S1H, S1I, and S1K), but no differences were detected in the percentage of monocytes or erythrocytes at either time point (Figures S1F, S1J, S1L, and S1M). When the DSS+WF group was included, it had similar effects compared to the DSS+FMD group. This group had significant reductions in lymphocyte count ($p < 0.0001$) (Figure S1H) and increases in granulocyte ($p < 0.01$) (Figure S1I), monocyte ($p < 0.0001$) (Figure S1J), and neutrophil levels ($p < 0.5$) (Figure S1K), with no changes in erythrocytes as noted before with the Naive, DSS, and DSS+FMD groups (Figure S1M).

We evaluated gut permeability by measuring the concentration of fluorescein isothiocyanate (FITC)-dextran in the serum. FMD

(E) The Hemoccult test variable of the DAI scores of the Naive (n = 15), DSS (n = 19), DSS+FMD (n = 18), and DSS+WF (n = 11) groups starting after the third DSS cycle.
(F) Visual representation of Hemoccult test results for Naive group (0), after 3 cycles of DSS (1), after 4 cycles of DSS (2), and after 4 cycles of DSS and 2 cycles of FMD (3). Blue color indicates presence of blood in stool.
(G) Visual representation of colon length from Naive, DSS control diet after 3 cycles (DSS 3 cycles), DSS control diet after four cycles (DSS 4 cycles), DSS control diet after 4 cycles of DSS plus 2 cycles of FMD (DSS+FMD) and DSS control diet plus 2 cycles of water-only fasting (DSS+WF) groups.
(H) Colon lengths of the Naive (n = 22), DSS 3 cycles (n = 6), DSS 4 cycles (n = 24), DSS+FMD (n = 23), and DSS+WF (n = 11) groups.
(I) Visual representation of small intestine from Naive, DSS 3 cycles, DSS 4 cycles, DSS+FMD, and DSS+WF groups.
(J) Small intestine lengths of the Naive (n = 8), DSS (n = 5), DSS+FMD (n = 5), and DSS+WF (n = 8) groups.
Data are presented as mean ± SEM; *$p < 0.05$, **$p < 0.01$, and ***$p < 0.001$, one-way or two-way ANOVA, and Bonferroni post test.
Related to Figure S1.

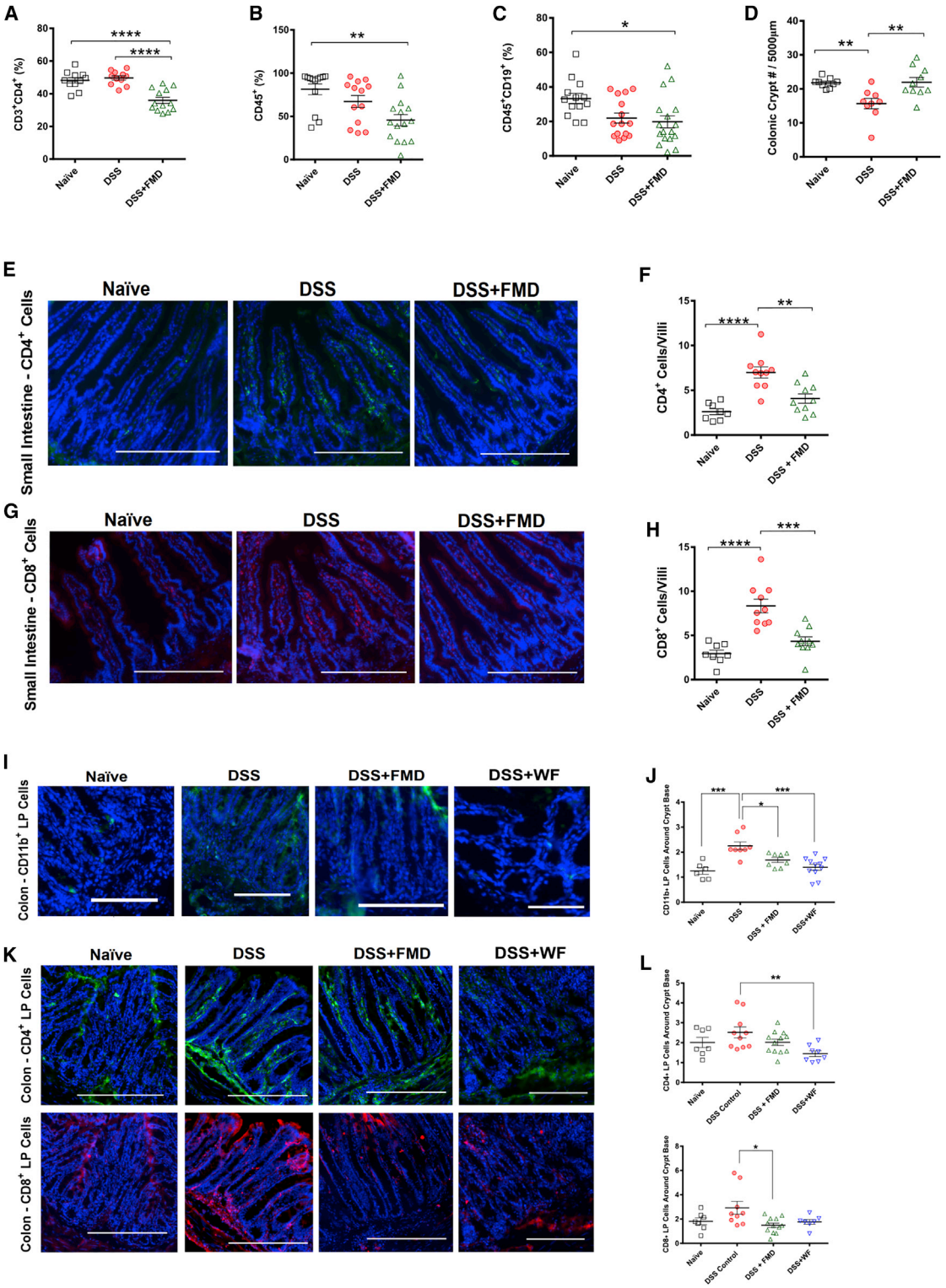

Figure 2. FMD Cycles Alter Immune Cell Profile to Reduce Intestinal Inflammation

(A) $CD4^+$ T cells ($CD3^+CD4^+$) in splenocytes of Naive (n = 11), DSS (n = 11), and DSS+FMD (n = 13) groups.

(B) $CD45^+$ leukocytes in splenocytes of Naive (n = 13), DSS (n = 13), and DSS+FMD (n = 15) groups.

(C) B Cells ($CD45^+CD19^+$) in splenocytes of Naive (n = 13), DSS (n = 15), and DSS+FMD (n = 17) groups.

(D) Colonic crypt number changes in Naive (n = 8), DSS (n = 9), and DSS+FMD (n = 10) groups.

(legend continued on next page)

cycles caused a return of the average FITC-dextran serum concentration to levels comparable to those observed in Naive mice, although neither the DSS-dependent increase nor the FMD-dependent decrease was significant ($p = 0.06$) (Figure S1N).

A reduction in colon length is a marker of intestinal damage after DSS treatment and a phenotypic feature used to assess IBD severity (Rose et al., 2012). After 4 DSS cycles, colon length was shortened to an average of 6.5 cm from an average of 7.6 cm in the Naive group ($p < 0.01$) (Figures 1G and 1H). When mice underwent 2 FMD cycles, colon length returned to normal ($p < 0.001$) (Figures 1G and 1H). Mice treated with 4 DSS cycles and that underwent two water-only fast cycles did not show improvements in colon length ($p < 0.05$) (Figure 1G). After 4 DSS cycles, the DSS+FMD but not the DSS+WF group displayed a significant increase in small intestine length compared to that in the DSS group ($p < 0.05$) (Figures 1I and 1J).

Overall, these data suggest that FMD cycles reversed several symptoms and pathology in a mouse model for IBD. In contrast, water-only fasting does not promote reversal of IBD-related pathology.

FMD Cycles Reduce Systemic and Intestinal Inflammation

To investigate the effects of FMD cycles on systemic inflammation in the chronic DSS mouse model, we monitored changes in splenocytes and peripheral blood mononuclear cells (PBMCs). Increased levels of circulating $CD4^+$ and $CD8^+$ T cells have been associated with IBD in patients, while a study in DSS-treated mice reported a modest increase in spleen $CD4^+$ T cells (Funderburg et al., 2013; Freise et al., 2018). In our study, DSS cycles did not cause an increase in $CD4^+$ T cells, but rather, we observed a significant reduction in the percentage of splenic $CD3^+CD4^+$ T cells in the DSS+FMD group compared to both the DSS and Naive groups ($p < 0.0001$) (Figure 2A). No differences in splenic $CD3^+CD8^+$ T cells were observed among the three groups (Figure S2E). Notably, the percentage of splenic $CD3^+CD4^+$ and $CD3^+CD8^+$ T cells that are central memory T cells (T_{CM}) was significantly higher in the DSS+FMD group compared to that in the Naive group ($p < 0.05$) (Figures S2F and S2G). In our study, the overall percentages of splenic $CD45^+$ leukocytes ($p < 0.01$; Figure 2B) and $CD45^+CD19^+$ B cells ($p < 0.05$; Figure 2C) were reduced in the DSS+FMD group compared to the Naive group. Although there were no changes in the percentage of splenic macrophages and monocytes among the three groups (Figures S2H and S2I), a significant increase in the percentage of myeloid cells was observed in the DSS+FMD group compared to the Naive group ($p < 0.05$) (Figure S2J). The percentage of splenic neutrophils was also significantly increased in both the DSS and the DSS+FMD groups when compared to that in the Naive group ($p < 0.05$ and $p < 0.01$, respectively) (Figure S2K). We also did not observe any changes in the percentage of $CD3^+CD4^+$ or $CD3^+CD8^+$ T cells, nor in the T_{CM} sub-type (Figures S2L and S2M), but we did detect a non-significant trend for a reduction in the overall percentage of $CD45^+$ leukocytes and $CD45^+CD19^+$ B cells in the DSS+FMD group (Figures S2N and S2O).

We assessed the severity of colon inflammation at the end of the study (Figure S2A). Although we did not observe a difference between the DSS and DSS+FMD groups, the DSS+FMD group showed a slight improvement compared to the DSS group (Naive versus DSS, $p < 0.0001$; Naive versus DSS+FMD, $p < 0.001$; Figure S2B). Also, four cycles of DSS caused a decrease in crypt number, which was reversed by 2 cycles of the FMD ($p < 0.01$; Figure 2D). It has been suggested that intestinal inflammation affects epithelium integrity and gut permeability (Landy et al., 2016). The increase in crypt number in the DSS+FMD group indicates that the elevated colonic inflammation score may be evidence of regenerative inflammation and not damaging inflammation (Eming et al., 2017).

Next, we investigated inflammatory markers in the intestinal tissue. We noticed a major increase in $CD4^+$ (Figure 2E) and $CD8^+$ cells (Figure 2G) in the small intestine villi of DSS-treated mice ($p < 0.0001$; Figure 2F and 2H), which was reversed by 2 FMD cycles ($p < 0.01$ and $p < 0.001$, respectively; Figures 2F and 2H). A characteristic of IBD is the accumulation of overactive dendritic cells at inflammation sites, which induce the differentiation of $CD4^+$ and $CD8^+$ effector lymphocytes that propagate at inflammation sites in the intestinal mucosa (Larmonier et al., 2015; Boschetti et al., 2016). In the colon, we analyzed $CD11b^+$ dendritic cells. These types of dendritic cells can drive type 2 T-helper lymphocyte (T_H2) responses, with the $CD11b^+CD103^-$ sub-population mediating these responses in the colon and the $CD11b^+CD103^+$ sub-population in the small intestine (Mayer et al., 2017). One study found increased numbers of $CD11b^+$ cells in the colonic lamina propria (LP) of mice predisposed to colitis (Ey et al., 2013). We found increased numbers of $CD11b^+$ cells in the colonic LP surrounding the base of crypts (Figure 2I) in the DSS group ($p < 0.001$; Figure 2J), which was lowered in the DSS+FMD group ($p < 0.05$; Figure 2J). The DSS+WF group also displayed a significant reduction in $CD11b^+$ cells compared to the DSS group ($p < 0.001$; Figure 2J). A similar pattern in the levels of $CD4^+$and $CD8^+$ cells was

(E) $CD4^+$ immunofluorescent (IF) staining in the small intestine of Naive, DSS, and DSS+FMD groups.
(F) $CD4^+$ cells per small intestinal villi in Naive (n = 8), DSS (n = 10), and DSS+FMD (n = 10) groups.
(G) $CD8^+$ IF staining in the small intestine of Naive, DSS, and DSS+FMD groups.
(H) $CD8^+$ cells per small intestinal villi in Naive (n = 8), DSS (n = 10), and DSS+FMD (n = 10) groups.
(I) $CD11b^+$ IF staining in the colon lamina propria of Naive, DSS, DSS+FMD, and DSS plus 2 cycles of water-only fasting (DSS+WF) groups.
(J) Colon lamina propria $CD11b^+$ cells around the crypt base of Naive (n = 6), DSS (n = 8), DSS+FMD (n = 8), and DSS+WF (n = 11) groups.
(K) $CD4^+$ and $CD8^+$ IF staining in the colon lamina propria of Naive, DSS, DSS+FMD, and DSS+WF groups.
(L) Colon lamina propria $CD4^+$ and $CD8^+$cells around the crypt base of Naive (n = 7), DSS ($CD4^+$, n = 10; $CD8^+$, n = 9), DSS+FMD (n = 12), and DSS+WF ($CD4^+$, n = 8; $CD8^+$, n = 7) groups.
Data are presented as mean ± SEM *$p < 0.05$, **$p < 0.01$, ***$p < 0.001$, and ****$p < 0.0001$, one-way ANOVA, and Bonferroni post test. IF images were taken at 20× magnification. Scale bar represents (E, G, and K) 200 μm and (I) 100 μm.
Related to Figure S2.

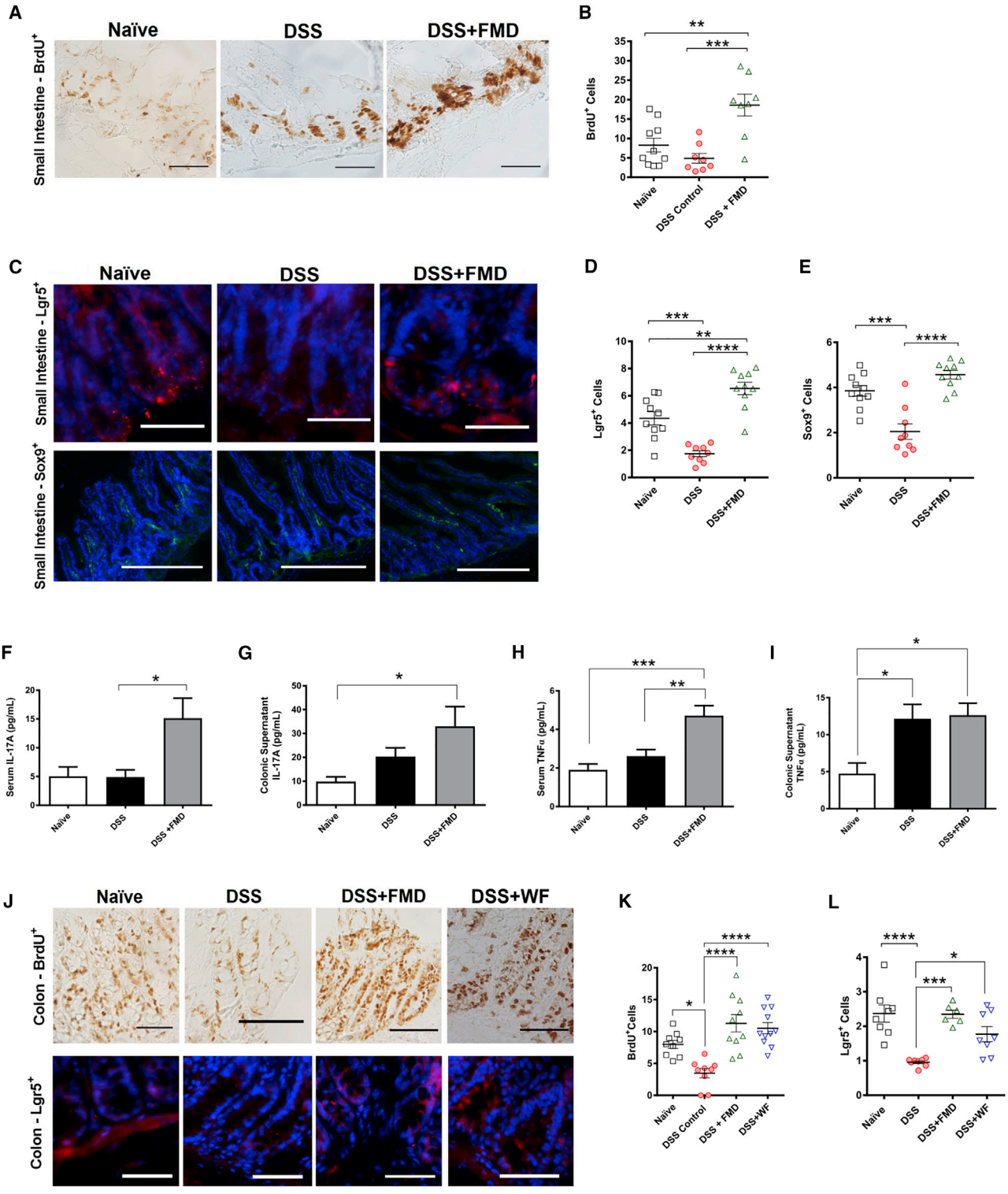

Figure 3. FMD Promotes Intestinal Regeneration

(A) Immunohistochemistry (IHC) for $BrdU^+$ cells in small intestine crypts of Naive, DSS, and DSS+FMD groups.

(B) $BrdU^+$ cells per small intestinal crypts in Naive (n = 10), DSS (n = 8), and DSS+FMD (n = 8) groups.

(C) Immunofluorescent (IF) staining for $Lgr5^+$ and $Sox9^+$ cells in the small intestine of Naive, DSS, and DSS+FMD groups.

(D) $Lgr5^+$ cells per small intestinal crypt in Naive (n = 10), DSS (n = 9), and DSS+FMD (n = 10) groups.

(legend continued on next page)

observed in the areas surrounding colonic crypts in the LP (Figures 2K and 2L). Regarding $CD8^+$ cells, only the DSS+FMD group showed a significant reduction when compared to the DSS group ($p < 0.5$; Figure 2L).

Taken together, the increase in colonic crypt number and reduction of $CD4^+$, $CD8^+$, and $CD11b^+$ cells in the intestinal epithelium support a role for FMD cycles in ameliorating intestinal inflammation in a mouse model for IBD.

FMD Cycles Promote Regeneration in the Gut and Small Intestine

Because gut regeneration could explain the reversal of the DSS-induced intestinal shortening by FMD treatment, we studied the effects of FMD cycles on markers of regeneration. We assessed small intestine regeneration by quantifying bromodeoxyuridine ($BrdU^+$) crypt cells (Figures 3A and 3B). The number of $BrdU^+$ cells per small intestinal crypt was increased in the DSS+FMD group when compared to the DSS and Naive groups ($p < 0.001$ and $p < 0.01$, respectively; Figure 3B). Previous studies have highlighted the protective quality of caloric restriction on ISC, indicated by the increase of $Lgr5^+$ stem cells and Paneth cells, the latter of which aids the self-renewing processes that occur in intestinal crypts (Tinkum et al., 2015; Yilmaz et al., 2012; Sato et al., 2011). Lgr5 is an established marker for crypt base columnar (CBC) stem cells (Barker, 2014), whereas Sox9 is expressed in CBCs but also in enteroendocrine cells (Formeister et al., 2009). We stained for Lgr5 and Sox9 (Figures 3C–3E) in the small intestine and observed a decrease in in the number of $Lgr5^+$ cells per crypt in DSS-treated mice ($p < 0.001$; Figure 3D), which was reversed by the FMD treatments ($p < 0.0001$; Figure 3D). Notably, the number of $Lgr5^+$ cells per crypt in the DSS+FMD group reached a level higher than that in Naive mice ($p < 0.01$; Figure 3D). Similarly, we detected a decrease in $Sox9^+$ cells in the upper-crypt spanning into the villus after 3 DSS cycles ($p < 0.001$; Figure 3E). Enteroendocrine cells can stimulate ISC division after exposure to a high-nutrient diet and may modulate ISC proliferation through the secretion of peptides, such as glucagon-like peptide-2 (GLP-2) (Amcheslavsky et al., 2014; Loudhaief and Gallet, 2016). FMD treatment promoted enteroendocrine-cell-dependent ISC regeneration, as determined by the expression of $Sox9^+$ cells in the intestinal villi ($p < 0.0001$; Figure 3E). In colonic crypts, DSS cycles also decreased the level of $BrdU^+$ cells ($p < 0.05$; Figure 3K), an effect reversed in the DSS+FMD group ($p < 0.0001$; Figure 3K). Colonic $BrdU^+$ cells were also increased in the DSS+WF group ($p < 0.0001$; Figure 3K). Similarly, DSS cycles decreased the number of $Lgr5^+$ cells in colonic crypts ($p < 0.0001$; Figure 3L); an effect reversed in both the DSS+FMD and DSS+WF groups ($p < 0.001$ and $p < 0.05$, respectively; Figure 3L).

Elevated levels of cytokines are associated with pro-inflammatory responses but could have a role in gut regeneration (Neurath, 2014; Karin and Clevers, 2016). We observed a significant increase in the serum cytokine level of interleukin-17A (IL-17A) in the DSS+FMD group when compared to the DSS group ($p < 0.05$; Figure 3F) and detected a similar increase in IL-17A in the colonic supernatant from the DSS+FMD group ($p < 0.05$; Figure 3G). Like IL-17A, tumor necrosis factor alpha (TNFα) also acts to enhance intestinal healing under inflammation-driven stress (Brockmann et al., 2017; Leppkes et al., 2014). Serum TNFα levels were greatly elevated in the DSS+FMD group when compared to both the DSS and Naive groups ($p < 0.01$ and $p < 0.001$, respectively; Figure 3H). TNFα in the colonic supernatant was elevated in both the DSS and DSS+FMD groups when compared to the Naive group, with no significant changes in colon tissue homogenate ($p < 0.05$; Figure 3I; Figure S2D). The role of interferon gamma (IFNγ) as a pro- or anti-inflammatory cytokine in the context of IBD is still a topic of debate (Conn, 2013). In our assessment of IFNγ in the serum and colonic supernatant for all three groups, we did not detect any significant changes (Figure S2C).

Overall, these results suggest that FMD cycles stimulate the generation of cytokines that may enhance the regenerative effects observed and increase the numbers of CBCs and enteroendocrine cells in the intestinal crypt that support gastrointestinal regeneration and repair.

FMD Cycles Stimulate an Increase in Microbial Populations Associated with T Cell Regulation and Gut Regeneration

To elucidate the potential role of microbiota in the effects of FMD cycles, we collected fecal stool samples from Naive mice or mice treated with 4 cycles of DSS±FMD (samples were collected 9 days after the 4^{th} DSS cycle and 2 days after the end of the 2^{nd} FMD cycle) (Figure 4A). After 4 DSS cycles, the overall microbiome composition was significantly altered in the DSS group, but the more pronounced changes occurred in the DSS+FMD group when compared to the DSS group (Figure 4B). The relative abundance of *S24-7* was down by more than two-fold (64.6% to 27.5% ± 7.9%; Table 1) and that of *Lactobacillaceae,* a family that regulates T cell activity and can reduce the severity of IBD symptoms in experimental models (Damaskos and Kolios, 2008), was increased three-fold (15.5% to 45.2% ± 4.2%; Table 1) in the

(E) $Sox9^+$ cells per small intestinal crypt-villi region in Naive (n = 10), DSS (n = 9), and DSS+FMD (n = 10) groups.
(F) Serum IL-17A levels (pg/ml) in Naive (n = 9), DSS (n = 14), and DSS+FMD (n = 16) groups.
(G) Colonic supernatant IL-17A levels (pg/ml) in Naive (n = 11), DSS (n = 17), and DSS+FMD (n = 18) groups.
(H) Serum TNFα levels (pg/ml) in Naive (n = 13), DSS (n = 20), and DSS+FMD (n = 27) groups.
(I) Colonic supernatant TNFα levels (pg/ml) in Naive (n = 12), DSS (n = 24), and DSS+FMD (n = 27) groups.
(J) IHC for $BrdU^+$ cells and IF staining for Lgr5+ cells in colonic crypts of Naive, DSS, DSS+FMD, and DSS+WF groups.
(K) $BrdU^+$ cells per colonic crypt in Naive (n = 9), DSS (n = 9), DSS+FMD (n = 10), and DSS+WF (n = 11) groups.
(L) $Lgr5^+$ cells per colonic crypt in Naive (n = 8), DSS (n = 8), DSS+FMD (n = 6), and DSS+WF (n = 8) groups.
Data are presented as mean ± SEM; *$p < 0.05$, **$p < 0.01$, ***$p < 0.001$, and ****$p < 0.0001$ one-way ANOVA, and Bonferroni post test. IF images were taken at 20× (40× for $BrdU^+$ cells of small intestine) magnification. Scale bar represents (A, C [$Lgr5^+$], and J) 100 μm and (C) 200 μm ($Sox9^+$).
Related to Figure S2.

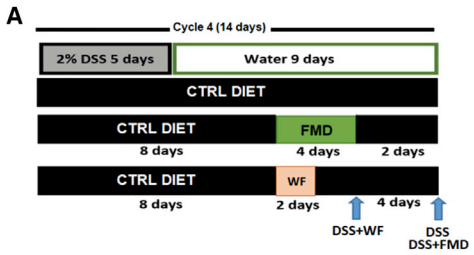

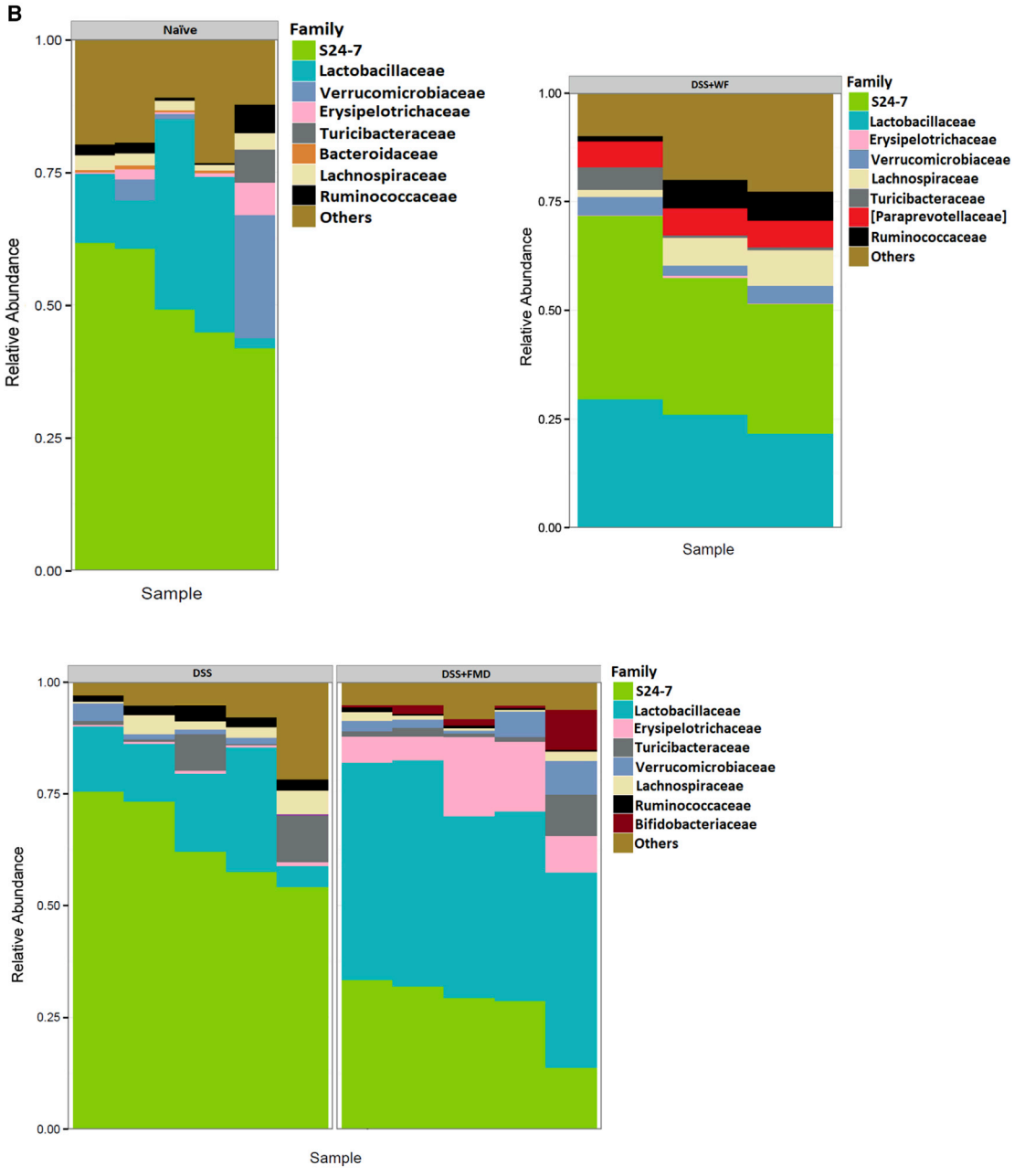

(legend on next page)

Table 1. Top 8 Most Abundant Families among the Naive, DSS, DSS+FMD, and DSS+WF Groups

Family	Naive Mean (SD)	DSS Mean (SD)	DSS+FMD Mean (SD)	DSS+WF Mean (SD)
S24-7	51.6 (9.08)	64.6 (9.46)	27.5 (7.9)	34.5 (6.72)
Lactobacillaceae	17.8 (14.2)	15.5 (8.36)	45.2 (4.2)	25.8 (3.97)
Erysipelotrichaceae	1.87 (2.41)	0.565 (0.226)	10.5 (5.71)	0.286 (0.184)
Turicibacteraeae	1.25 (2.78)	4.1 (4.83)	2.84 (3.63)	2.17 (2.59)
Verrucomicrobiaceae	5.65 (9.98)	1.57 (1.37)	3.65 (2.88)	3.5 (1.05)
Lachnospiraceae	2.18 (0.801)	2.83 (1.96)	1.16 (0.756)	5.42 (3.32)
Ruminococcaceae	2.09 (1.97)	2.36 (0.783)	0.568 (0.308)	4.81 (3.09)
Bacteroidaceae[a]	0.409 (0.257)	–	–	–
Bifidobacteriaceae[b]	–	0.0346 (0.0384)	2.67 (3.56)	–
[*Paraprevotellaceae*][c]	–	–	–	6.13 (0.148)

Related to Figures 4 and S3 and Tables S1–S6.
[a]Not ranked in top 8 most abundant families for DSS, DSS+FMD, and DSS+WF groups.
[b]Not ranked in top 8 most abundant families for Naive and DSS+WF group.
[c]Not ranked in top 8 most abundant families for Naive, DSS, and DSS+FMD groups.

DSS+FMD compared to DSS group. *Bifidobacteriaceae,* a microbial family that has been shown to ameliorate symptoms in DSS-colitis models (Srutkova et al., 2015), was found to be uniquely enriched in the DSS+FMD group (0.034% to 2.67% ± 3.56%; Table 1). We also observed a significant increase in the relative abundance of *Erysipelotrichaceae* (10.5% ± 5.71%; Table 1) in the DSS+FMD group, although the role of this family in the context of IBD is still not clear (Kaakoush, 2015). Of this family, the genus *Allobaculum* was enriched in the DSS+FMD group (data not shown). *Allobaculum* has been associated with protection from obesity and insulin resistance, with one study finding its relative abundance to be increased alongside *Bifidobacterium* in mice with a lean phenotype (Everard et al., 2014; Raza et al., 2017). After the 2nd water-only fast and 2 days of re-feeding, the DSS+WF group had a small increase in *Lactobacillaceae* (25.8% ± 3.97%; Table 1; Figure 4B); however, *Bifidobacteriaceae* was undetectable (Table 1). *Paraprevotellaceae* was detected only in the DSS+WF group (6.13% ± 0.148%; Table 1). The Naive, DSS, DSS+FMD, and DSS+WF groups separated according to group and time point (Table S6; Figure S7A, p = 0.001; Figure S7D, p = 0.001; Figure S7E, p = 0.014).

We also compared the composition of the most abundant families between the groups at different time points (Figure S3A; Table S1). Two days after the 4th cycle of DSS and one day before the 2nd FMD cycle, the DSS and DSS+FMD groups did not display major changes in microbiota composition (Figure S3B; Table S2). When we compared the DSS+FMD group one day before the 2nd FMD cycle versus on the last day of the 2nd FMD cycle, we observed a reduction in the relative abundance of *S24-7* and an increase in *Erysipelotrichaceae*, and a significant decrease in *Lactobacillaceae* abundance (Figure S3C; Table S3). Despite the temporary reduction at the end of the FMD cycle, the *Lactobacillaceae* levels increased approximately 45-fold after 2 days of re-feeding with the normal diet after the 2nd FMD cycle (Figure S3E; Table 1; Table S3), indicating that the major microbiota changes require both the FMD and several days of re-feeding with a normal diet.

The abundance of *Erysipelotrichaceae* was approximately 4-fold lower between the mice on the last day of the 2nd water-only fast and those on the last day of the 2nd FMD cycle (23% to 6.16% ± 4.83%; Table S4; Figure S3Dd). A striking difference between the microbiomes of these groups was also the presence of *Paraprevotellaceae,* which was more abundant than *Lactobacillaceae* in the water-only fasting group compared to the FMD group (12.9% ± 3.41% versus 5.77% ± 1.18%; Table S4; Figure S3D). On the last day of the 2nd water-only fasting and FMD cycles, samples separated at a significant p value in the weighted ordination (p = 0.033; Table S6; Figure S7F). The samples of the DSS and DSS+FMD groups, 2 days after the 4th DSS cycle and 1 day before the 2nd FMD cycle, did not separate at a significant value (p = 0.579; Table S6; Figure S7B). When two time points of the DSS+FMD group were compared, 1 day before the 2nd FMD cycle and on the last day of the 2nd FMD cycle, samples did not separate at a significant p value in the weighted ordination (p = 0.265; Table S6; Figure S7c).

These results indicate that FMD cycles increase the abundance of protective microbial families, such as *Lactobacillaceae* and *Bifidobacteriaceae*, while also altering the abundance of other microbial strains to restore a protective gut microbiome in DSS-treated mice.

Figure 4. FMD Stimulates an Increase in Microbial Strains Known to be Associated with T Cell Regulation and Gut Regeneration
(A) Fecal samples were collected from the Naive, DSS, DSS+FMD, and DSS+WF groups after 4 cycles of DSS and 2 cycles of FMD or 2 cycles of water-only fasting.
(B) Plot summarizing the composition of most abundant microbial families in fecal samples from the Naive (n = 5), DSS (n = 5), DSS+FMD (n = 5), and DSS+WF (n = 3) groups.
Data were compiled by Second Genome Solutions using the 16S V4 rRNA gene sequencing on the Illumina MiSeq platform.
Related to Figures S3 and S7 and Tables S1–S4 and S6.

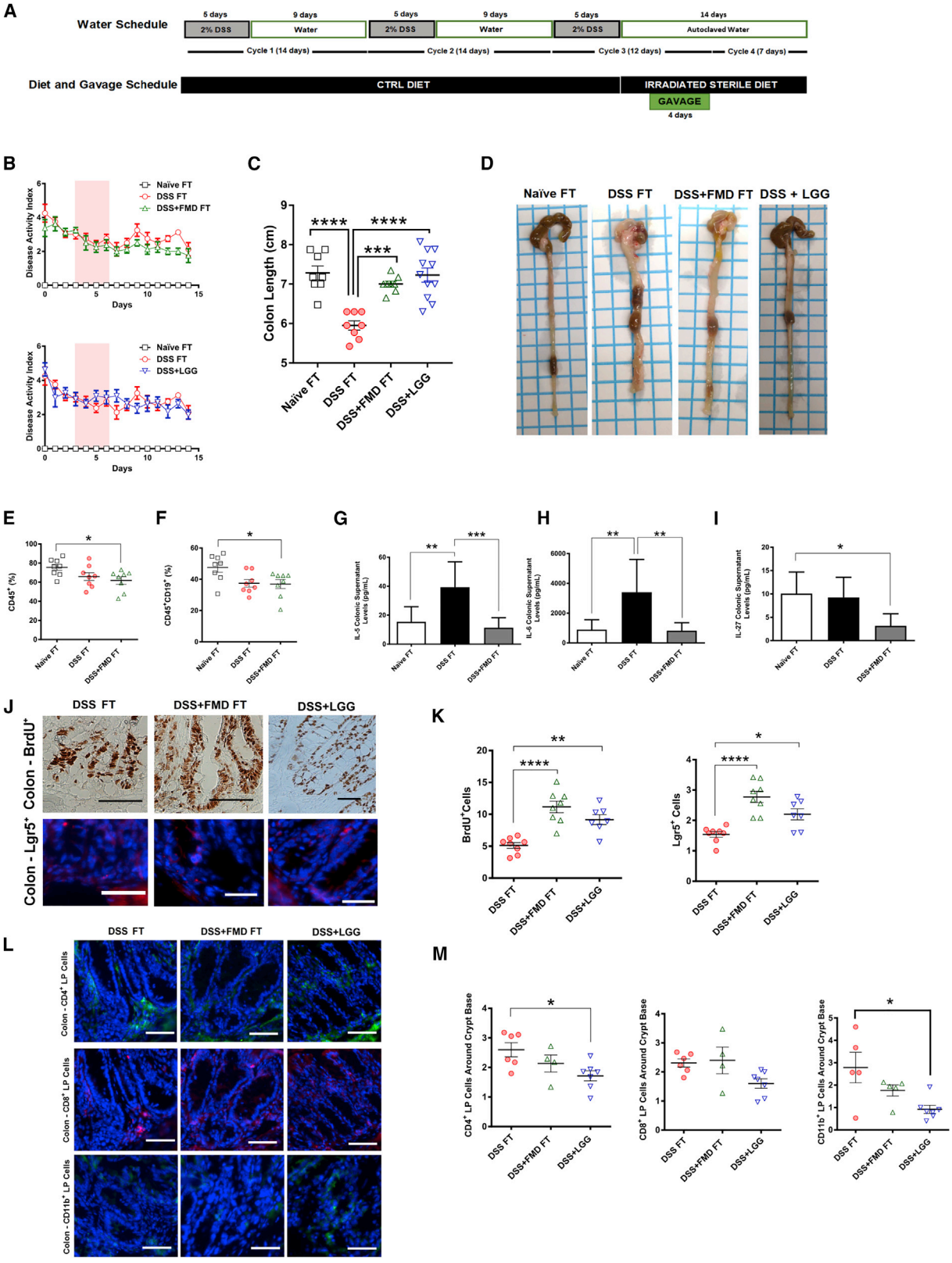

(legend on next page)

Fecal Transplant from FMD-Treated Mice Promotes Positive Changes in IBD-Associated Symptoms

To investigate whether the shift in the microbiome is responsible for the effects of the FMD on IBD-associated pathology, we performed a fecal transplant (Figure 5A) (Ellekilde et al., 2014). Recipient mice were divided into three groups: a group that received no DSS, but a 1:1 control gavage solution of sterile PBS and glycerol during the gavage period (Naive FT), a group that received three DSS cycles and a cecum-derived solution from mice in the DSS group (DSS FT), and a group that received three DSS cycles and a cecum-derived solution from mice in the DSS+FMD group (DSS+FMD FT). Another group underwent three DSS cycles and a gavage treatment of the *Lactobacillus* strain, *Lactobacillus rhamanosus* (LGG) (DSS+LGG). We measured IBD DAI every day starting on the last day of the 3rd DSS cycle (Figure 5B). The DSS+FMD FT group showed a non-significant trend for a lower DAI score than that in the DSS FT group, 2–3 days after the last day of gavage, whereas the DSS+LGG group did not display a significant change in the overall and sub-DAI scores compared to the DSS FT group (Figure 5B; Figures S4A–S4C).

We observed a reduction in colon length in the DSS FT group when compared to the Naive FT (Figure 5C; $p < 0.0001$, Figure 5D) and a return to the normal colon length in the DSS+FMD FT and DSS+LGG groups when compared to the DSS FT group (Figure 5C; $p < 0.001$, Figure 5D). The white blood cell composition from whole blood at the end of the experiment did not show major changes (Figures S5A, S5B, and S5D), except for an increase in monocytes in the DSS+LGG group compared to the DSS FT and DSS+FMD FT groups (Figure S5C; $p < 0.05$) and a decrease in erythrocyte volume compared to the Naive FT, DSS FT, and DSS+FMD FT groups (Figure S5E; $p < 0.001$). Splenic CD45$^+$ leukocytes and B cells in the DSS+FMD FT group were reduced compared to the Naive FT group ($p < 0.05$; Figure 5E; Figure 5F). Splenic neutrophils were increased in both the DSS FT and DSS+FMD groups ($p < 0.01$; Figure S5F). Splenocyte CD4$^+$ T cells were not affected, but we did see a reduction of CD8$^+$ T cells in both recipient groups and an increase in the percentage of the CD8$^+$ T cells of the T_{CM} subtype for both groups, ($p < 0.01$ and $p < 0.05$, respectively; Figures S5G and S5H).

IL-5 and IL-6 are significantly elevated in UC patients (Olsen et al., 2011), and although we did not observe any changes in serum levels of IL-5 and IL-6 (Figures S5I and S5J), the DSS FT group displayed higher levels of both cytokines in colonic supernatant when compared to those from Naive FT controls, which were reduced in the colonic supernatant from the DSS+FMD FT group ($p < 0.001$, $p < 0.01$, and $p < 0.01$, respectively; Figures 5G and 5H). IL-23 and IL-27 are cytokines thought to be activated in CD, with IL-23 involved in T_H17 differentiation (Sartor, 2006). CD patients have been reported to have increased serum IL-27, but this cytokine may have anti-inflammatory functions due to its ability to trigger IL-10 production (Andrews et al., 2016). IL-23 and IL-27 were increased in the serum of the DSS+FMD FT group ($p < 0.05$; Figures S5K and S5L), whereas IL-27 was reduced in the colonic supernatant, which was evident in the DSS+FMD FT group ($p < 0.05$; Figure 5I). There were no changes among groups in the colonic supernatant levels of IL-23 (Figure S5M).

Additionally, we measured several cytokines associated with CD or colitis in distal colon tissue homogenate from the FT groups (Figure S5N). IFNγ was elevated in the DSS+FMD FT group compared to the Naive FT control ($p < 0.05$; Figure S5N), as was IL-17A ($p < 0.01$; Figure S5N). The DSS+FMD FT groups had higher levels of TNFα than the DSS FT group ($p < 0.05$; Figure S5N). Its consistent increase in the DSS+FMD FT group was in agreement with what we found with the DSS+FMD group (Figures 3F–3I). There were no changes in IL-13, but for IL-10, an anti-inflammatory cytokine and immunoregulator of T_H2 responses (Couper et al., 2008), we found that compared to the Naive FT control, the DSS FT group displayed a lower level in colonic tissue ($p < 0.01$; Figure S5N), whereas the DSS+FMD FT caused a trend for a reversal of this effect (Figure S5N, Naive FT versus DSS+FMD FT group; $p < 0.05$).

Figure 5. Fecal Transplant from FMD-Treated Mice Improves IBD-Associated Phenotypes, Alters Immune Cell Profile, Stimulates Regeneration in the Colon, and Reduces Levels of Cytokines Associated with IBD Pathogenesis

(A) Experimental scheme outlining the water schedule, duration of diet, and transplant gavage.

(B) The modified DAI scores (with body weight loss removed) of the mice that received a control PBS-glycerol solution (Naive FT), mice that received 3 DSS cycles and a cecum-derived solution from mice in the DSS group (DSS FT), 3 that received three DSS cycles and a cecum-derived solution from mice in the DSS+FMD group (DSS+FMD FT), and mice that received three DSS cycles and a gavage treatment of the *Lactobacillus* strain *Lactobacillus rhamanosus* (DSS+LGG) groups starting after the third DSS cycle through the 4-day gavage treatment. Pink background represents period of gavage treatment.

(C) Colon lengths of the Naive FT, DSS FT, DSS+FMD FT, and DSS+LGG groups.

(D) Visual representation of colon length from the Naive FT, DSS FT, DSS+FMD FT, and DSS+LGG groups after 3 cycles of DSS, 4 days of transplant gavage, and a 1-week respite period.

(E) CD45$^+$ leukocytes in splenocytes of Naive FT, DSS FT, and DSS+FMD FT groups.

(F) B Cells (CD45$^+$CD19$^+$) in splenocytes of Naive FT, DSS FT, and DSS+FMD FT groups.

(G) Colonic supernatant IL-5 levels (pg/ml) in Naive FT (n = 7), DSS FT (n = 7), and DSS+FMD FT groups.

(H) Colonic supernatant IL-6 levels (pg/ml) in Naive FT (n = 7), DSS FT, and DSS+FMD FT groups.

(I) Colonic supernatant IL-27 levels (pg/ml) in Naive FT, DSS FT (n = 7), and DSS+FMD FT (n = 4) groups.

(J) IHC for BrdU$^+$ cells and IF staining for Lgr5+ cells in colonic crypts of the DSS FT, DSS+FMD FT, and DSS+LGG groups.

(K) BrdU+ and Lgr5+ cells in colonic crypts of the DSS FT, DSS+FMD FT, and DSS+LGG (BrdU$^+$ and Lgr5$^+$, n = 7) groups.

(L) IF staining for CD4$^+$, CD8$^+$, and CD11b$^+$ colon lamina propria cells of the DSS FT, DSS+FMD FT, and DSS+LGG groups.

(M) Colon lamina propria CD4$^+$, CD8$^+$, and CD11b$^+$ around the colonic crypt base of the DSS FT (CD4$^+$, n = 6; CD8$^+$, n = 6; CD11b$^+$, n = 5), DSS+FMD FT (CD4$^+$, n = 4; CD8$^+$, n = 4; CD11b$^+$, n = 5), and DSS+LGG (n = 7) groups.

Data are presented as mean ± SEM; *$p < 0.05$, **$p < 0.01$, ***$p < 0.001$, and ****$p < 0.0001$, one-way ANOVA, and Bonferroni post test. n = 8/group unless otherwise noted. Scale bar represents (J) 100 μm (BrdU$^+$) and (J [Lgr5$^+$] and L) 50 μm.

Related to Figures S4 and S5.

We also evaluated the expression of specific regenerative and inflammatory markers (Figures 2 and 3). $BrdU^+$ analysis revealed a significant increase in BrdU+ cells in colonic crypts in both the DSS+FMD FT and DSS+LGG groups, when compared to the DSS FT group. Figure 5J refers to the microscopy images, and Figure 5K shows the quantification of BrdU ($p < 0.0001$ [DSS+FMD FT versus DSS FT] and $p < 0.01$ [DSS+LGG versus DSS FT]). A similar increase was seen in colonic $Lgr5^+$ cells in the crypts of the DSS+FMD FT and DSS+LGG groups. Figure 5J refers to the microscopy images, and Figure 5J shows the quantification of Lgr5+ ($p < 0.0001$ [DSS+FMD FT versus DSS FT] and $p < 0.05$ [DSS+LGG versus DSS FT]). In the LP cells surrounding the base of colonic crypts, the DSS+LGG group displayed a reduction in $CD4^+$ and $CD11b^+$ cells when compared to the DSS FT group, whereas the DSS+FMD FT group showed a trend toward a reduction in the levels of these cells (Figure 5L; $p < 0.05$; Figure 5M), but neither of the three groups showed changes in $CD8^+$ cells. Certain strains of *Lactobacillus* tend to suppress T_H2 responses, and because $CD11b^+$ cells have been observed to drive T_H2 responses in the colon. It is plausible from these results that *Lactobacillus* works to suppress T_H2 responses in the colon by reducing $CD11b^+$ levels (Mayer et al., 2017).

We also investigated which microbial families were present after a fecal transplant (Figure S6A). Samples for the three groups showed different profiles according to the treatment group (Table S6; DSS+FMD versus DSS+FMD FT, $p = 0.007$, Figure S7G; DSS+FMD versus DSS+LGG, $p = 0.009$, Figure S7H). Interestingly, microbiota form both the DSS+FMD FT and DSS+LGG groups did not have as high of an abundance of *Lactobacillaceae* as the DSS+FMD group (DSS+FMD versus DSS+FMD FT, 45.3% ± 4.18% versus 12.2% ± 12.1%; DSS+FMD versus DSS+LGG, 45.3% ± 4.8% versus 7.18% ± 3.95%; Table S5), although the DSS+FMD FT group displayed an enrichment of the *Lactobacillus crispatus* and *Lactobacillus intestinalis* strains (data not shown). Notably, both the DSS+FMD FT and DSS+LGG groups showed an increase in the *Verrucomicrobiaceae* family compared to the DSS+FMD group (DSS+FMD versus DSS+FMD FT, 3.64% ± 2.87% versus 10.5% ± 5.1%; DSS+FMD versus DSS+LGG, 3.64% ± 2.87% versus 5.99% ± 4.79%; Table S5). Upon further analysis, both groups were found to be enriched with the strain *Akkermansia muciniphila*, a mucin-degrading bacterium that has been linked to reduced intestinal inflammation and strengthening the epithelial gut barrier (Reunanen et al., 2015). The *Bacteroidaceae* family was very abundant in the DSS+FMD FT group when compared with the DSS+FMD and DSS+LGG groups (17.7% ± 11%; Table S5), although the *Bacteroides acidifaciens* strain was found to be enriched in both the DSS+FMD and DSS+FMD FT groups (data not shown). Although the bacterial family *Rikenellaceae* was not ranked in the top 8 or 9 families among the DSS+FMD, DSS+FMD FT, and DSS+LGG groups (Table S5), the strain *Alistipes shahii*, which belongs to the *Rikenellaceae* family, was uniquely enriched in the DSS+LGG group (data not shown) and is reported to modulate tumor growth in the gut (Belkaid and Hand, 2014).

These results indicate that FMD cycles cause shifts in gut microbiota populations that, in turn, affect the immune cell profile, cytokine levels, and regenerative activity in the colon.

FMD Cycles Reduce IBD-Associated Inflammation in Humans and Mice, in Part, by Modulating White Blood Cell Counts

C-reactive protein (CRP) is an established marker for inflammatory diseases, including IBD, in human subjects (Vermeire et al., 2006; Henriksen et al., 2008). We have previously shown that 3 FMD cycles reduce CRP levels in subjects with elevated CRP at baseline (Wei et al., 2017). Here, we analyzed serum samples of mice that received 3 DSS cycles and observed a non-significant trend for an increase in lymphocyte count (Figure 6D) and a significant increase in lymphocyte percentage (Figure S1C) but not in white blood cell (WBC) count (Figure 6C). Both at the end of the first FMD cycle and two days after the 2^{nd} FMD cycle post-DSS treatment, lymphocyte counts were reduced when compared to both Naive mice and mice that underwent 4 DSS cycles on a standard diet (Figure 6D; Naive versus B $p < 0.01$; A versus B, $p < 0.001$). A non-significant trend for a reduction in WBCs was also observed after FMD treatments (Figure 6C).

We analyzed the levels of WBCs and lymphocytes, and the effect of 3 cycles of a 5-day FMD on them in human subjects with elevated CRP (>1 mg/L) (Wei et al., 2017). In subjects with elevated CRP, the WBC counts were increased compared to those in subjects with CRP in the normal range (<1 mg/L). These were reduced at the end of FMD cycle 1, as well as after 3 FMD cycles (Figure 6A; $p < 0.05$). A reduction in lymphocytes was also apparent at the end of FMD cycle 1 for the higher CRP group (Figure 6B; $p < 0.05$), but after completing 3 FMD cycles, the lymphocytes of the higher CRP group had returned to levels not different from those at baseline (Figure 6B).

These results suggest that FMD cycles can reduce systemic inflammation and the associated increase in lymphocyte counts or percentage in both mice and humans. A randomized clinical trial on IBD patients is necessary to test the hypothesis that FMD cycles reduce IBD pathology in humans.

DISCUSSION

Dietary interventions that promote coordinated beneficial changes in the hematopoietic and immune systems, and especially in the gut microbiota, have high potential to ameliorate and possibly reverse CD, colitis, and other inflammatory and autoimmune diseases. In this study, using the chronic DSS model for IBD, we show that two cycles of a 4-day FMD followed by a normal diet are sufficient to mitigate some, and reverse other, IBD-associated pathologies or symptoms. In contrast, water-only fasting only causes some of the effects of the FMD cycles, indicating that certain nutrients in the FMD contribute to the microbial and anti-inflammatory changes necessary to maximize the effects of the fasting regimen. The lack of a significant change in the stool consistency and Hemoccult scores in the water-only group could be explained by the complete lack of nutrients. In fact, diets low or lacking carbohydrates and dietary fibers have been shown to significantly decrease colonic cancer-protective fecal metabolites and exacerbate colitis, prolonging symptoms like bloody stools, with mitigation of symptoms seen after switching to a plant-based and semi-vegetarian diet (Russell et al., 2011; Chiba et al., 2016). The FMD itself contains prebiotic ingredients based on the same high-fiber

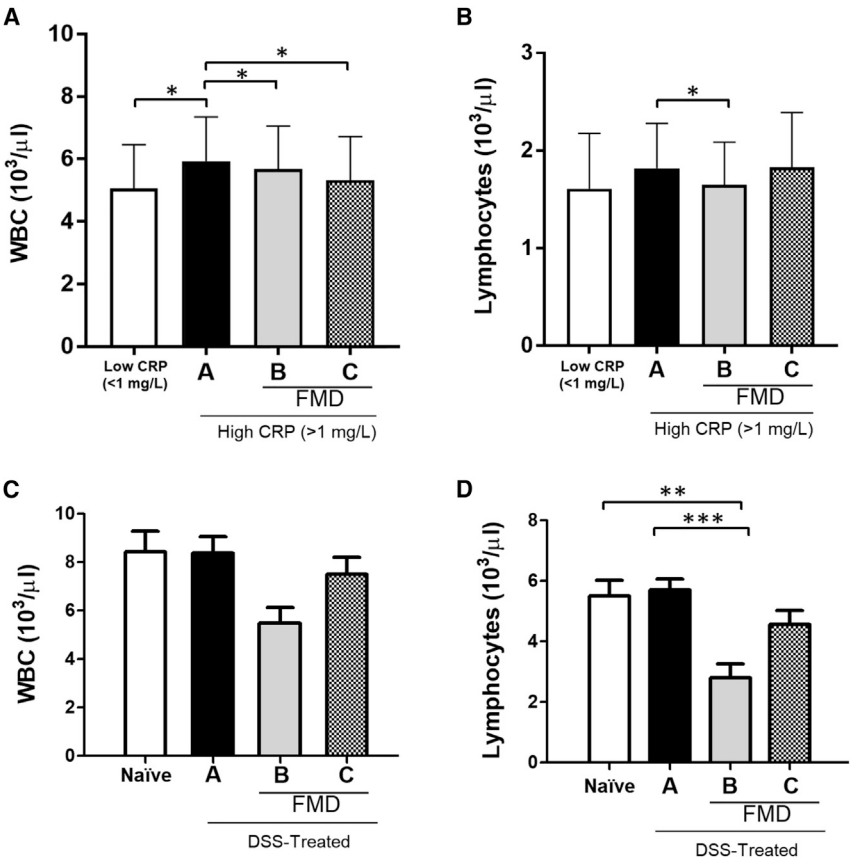

Figure 6. White Blood Cell (WBC) and Lymphocyte Counts in Humans and Mice with Systemic Inflammation

(A) WBC count ($10^3/\mu l$) from patients with low CRP (< 1 mg/L; n = 36) or higher CRP (>1 mg/L) prior to dietary intervention (a) (n = 25), at the end of an initial 5-day FMD cycle before resuming normal food intake (b) (n = 25), and approximately 5 days after completing 3 FMD cycles and refeeding (c) (n = 25).

(B) Circulating lymphocyte count ($10^3/\mu l$) from patients with low CRP (<1 mg/L; n = 36) or high CRP (>1 mg/L) prior to dietary intervention (a) (n = 25), at the end of an initial 5-day FMD cycle before resuming normal food intake (b) (n = 25), and approximately 5 days after completing 3 FMD cycles and refeeding (c) (n = 25).

(C) WBC counts ($10^3/\mu l$) in untreated, naive mice (n = 14) or mice that received 4 cycles of DSS (a) (n = 19), on the last day of 1 cycle of a 4-day FMD between the 3rd and last DSS cycles (b) (n = 9), and two days after 4 DSS cycles and 2 FMD cycles (c) (n = 18).

(D) Circulating lymphocyte counts ($10^3/\mu l$) in untreated, naive mice (n = 14) or mice that received 4 cycles of DSS (a) (n = 19), on the last day of 1 cycle of a 4-day FMD between the 3rd and last DSS cycles (b) (n = 9), and two days after 4 DSS cycles and 2 FMD cycles (c) (n = 18). Data are presented as mean ± SEM; *p < 0.05, **p < 0.01, and ***p < 0.001, one-way ANOVA, and Bonferroni post test.

ingredients used in the FMD human clinical trials (Wei et al., 2017), such as oligofructoses, fructo-oligosacharides, and galactomannan, derived from vegetables that can support the growth of beneficial probiotic strains (Gibson et al., 2017; Markowiak and Śliżewska, 2017).

Short, water-only fasting has been shown to prevent and help treat intestinal inflammation in acute DSS models (a single, 5-day DSS treatment) (Sävendahl et al., 1997; Okada et al., 2017). Our study, using the chronic DSS model that more closely reflects the symptoms and pathology associated with IBD, indicates that fasting alone is not sufficient to reverse the pathology associated with IBD, but it is its combination with certain ingredients that is effective. Also, the FMD treatment in the current study lasts 4 days and is repeated multiple times, compared to the single, water-only fasting lasting between 36–48 hours in previous studies. Notably, *Paraprevotellaceae*, associated with water-only fasting but not FMD treatment, has been previously regarded as pro-inflammatory in the context of IBD, with one study finding it to be especially enriched in mice with severe colitis (Roy et al., 2017). Another study also found *Paraprevotellaceae* abundance increased in rats with increased pro-inflammatory cytokines, such as IL-13, in colonic tissue (Shatzkes et al., 2017).

Our results also indicate that the growth and replacement of damaged intestinal tissues occur strongly during the re-feeding post-FMD, although our previous studies in multiple tissues indicate that stem and other progenitor cells are activated already during the FMD. This process may help explain the increased expression of IL-17A in the FMD group. In fact, the intestinal epithelium damage caused by the IBD state is thought to trigger higher levels of FGF-2, a propagator of ISC regeneration, which works with IL-17A to promote mucosal healing and intestinal epithelial cell proliferation (Brockmann et al., 2017; Houchen et al., 1999). Also, in clinical trials and studies with colitis mouse models, anti-IL-17A treatments aggravate IBD-associated symptoms, suggesting that IL-17A may play a role in reducing intestinal inflammation and promote gut healing (Whibley and Gaffen, 2015). TNFα has been previously reported to be chronically elevated in IBD patients, and TNFα inhibitors, such as infliximab and adalimumab, have long been established as effective treatments for IBD patients (Lichtenstein, 2013). One possible interpretation of the effects of the FMD on increasing TNFα in our study is that TNFα has both functions that are detrimental and those that are beneficial. In fact, TNFα is well-established to promote cell death but also promote wound healing and immune cross-talk (Leppkes et al., 2014). In agreement with our previous studies, we hypothesize that FMD cycles can first reduce the inflammation associated with IBD initiated by DSS treatment and, subsequently, promote regeneration during the re-feeding stage. Thus, the intestinal inflammation leading to crypt hypertrophy with enhanced epithelial proliferation observed in humans is consistent with our findings and hypothesis that the FMD can turn this disease-associated inflammatory state into a regenerative process.

It was originally proposed that DSS-induced inflammation does not involve lymphocytes; however, later studies have suggested that immunity may play a role in the pathogenesis of the DSS-induced model. One study using Rag1-knockout (KO) mice found that when DSS was administered, the immunodeficient mice actually had a slower, more tolerable progression in disease symptoms than that of control mice, suggesting T and/or B cells may contribute to pathology progression (Kim et al., 2006). Another study also supports an increased inflammatory and immune response in the DSS model (Morgan et al., 2013), indicating that although the use of IL-10 KO and similar mice can more strongly model autoimmune IBD, the DSS model may better model environmentally induced IBD. Notably, the DSS model also avoids the concern that if the FMD or other treatments required elevated IL-10, their effects would not be observed.

In summary, these results indicate that cycles of FMD and refeeding can ameliorate or reverse the symptoms and pathology associated with IBD in a chronic DSS mouse model in part through modulation of the gut microbiome. These FMD cycles also reduce lymphocyte number and intestinal infiltration, increase intestinal regeneration in DSS-treated mice, and lower multiple markers of systemic inflammation in humans. These promising results justify the testing of FMD cycles in randomized clinical trials as a therapy for CD and colitis.

STAR★METHODS

Detailed methods are provided in the online version of this paper and include the following:

- KEY RESOURCES TABLE
- CONTACT FOR REAGENT AND RESOURCE SHARING
- EXPERIMENTAL MODEL AND SUBJECT DETAILS
  - Mouse Models
  - Chronic dextran sodium sulfate (DSS)-induced mouse model
  - Fecal transplant and Lactobacillus transplant models
  - Human FMD trial
  - Criteria for inclusion of human subjects
  - Exclusion criteria
  - Profile
- METHOD DETAILS
  - Mouse fasting mimicking diet
  - Post-diet refeeding
  - DAI scoring
  - Colon inflammation score
  - BrdU Injection
  - Immunohistochemistry analysis
  - FACS Analysis
  - Cytokines profiling
  - FITC Dextran Permeability
  - Microbiome sequencing
  - Human fasting-mimicking diet
  - Ingredients
  - Supplements
- QUANTIFICATION AND STATISTICAL ANALYSIS
- ADDITIONAL RESOURCES

SUPPLEMENTAL INFORMATION

Supplemental Information includes seven figures and five tables and can be found with this article online at https://doi.org/10.1016/j.celrep.2019.02.019.

ACKNOWLEDGMENTS

We thank Marco Colonna at Washington University, St. Louis, for the careful review of the manuscript and suggestions. We thank Bernadette Masinsin (USC Flow Cytometry Core Facility) for assistance with the BD FACS Diva/LSR II; Luisa Chan, Cheryl Chow, and Nicole Narayan (Second Genome Solutions) for help with analysis of microbiome sequencing data; Louis Dubeau (USC/Norris Comprehensive Cancer Center) for assistance with inflammation scoring; Damon Cook (Thermo Fisher) for assistance in the cytokine profiling; and Arjun Reddy, Victoria Hahn, Dolly Chowdhury, Kyle Xia, Claire Nguyen, Arjun Reddy, Chae Sutherland, Katelynn Tran, Kevin Soleimani, Cheyenne Schloffman, and Melissa Carpenter for their technical assistance. This study was funded in part by NIH/NIA grants AG20642, AG025135, P01 AG055369, and P01 AG034906 and the Glenn Foundation for Medical Research (GFMR) to V.D.L.

AUTHOR CONTRIBUTIONS

P.R., I.Y.C., M.W., and V.D.L. designed mouse experiments. P.R. and I.Y.C. performed the mouse experiments. P.R. and G.N. performed tissue collection. G.N. prepared mouse FMD. P.R., N.E., G.P., D.M., M.A., and V.O. performed and processed immunohistochemistry and quantitative analysis. P.R., M.A., and V.O. processed tissue for fluorescence-activated cell sorting (FACS). I.Y.C. and E.G. conducted FACS analysis. P.R. performed cytokine assays. S.B. collected and analyzed human clinical trial data. P.R. and V.D.L. wrote the manuscript with input from I.Y.C., S.B., and M.W.

DECLARATION OF INTERESTS

V.D.L. has equity interest in L-Nutra, which develops and sells medical food for the prevention and treatment of diseases. V.D.L. has committed all his equity in the company to charitable organizations. V.D.L., P.R., and I.Y.C. have filed a patent related to this study at the University of Southern California (USC).

Received: November 8, 2018
Revised: January 1, 2019
Accepted: February 6, 2019
Published: March 5, 2019

REFERENCES

Amcheslavsky, A., Song, W., Li, Q., Nie, Y., Bragatto, I., Ferrandon, D., Perrimon, N., and Ip, Y.T. (2014). Enteroendocrine cells support intestinal stem-cell-mediated homeostasis in Drosophila. Cell Rep. *9*, 32–39.

Andrews, C., McLean, M.H., and Durum, S.K. (2016). Interleukin-27 as a novel therapy for inflammatory bowel disease. Inflamm. Bowel Dis. *22*, 2255–2264.

Barker, N. (2014). Adult intestinal stem cells: critical drivers of epithelial homeostasis and regeneration. Nat. Rev. Mol. Cell Biol. *15*, 19–33.

Belkaid, Y., and Hand, T.W. (2014). Role of the microbiota in immunity and inflammation. Cell *157*, 121–141.

Boschetti, G., Nancey, S., Moussata, D., Cotte, E., Francois, Y., Flourié, B., and Kaiserlian, D. (2016). Enrichment of circulating and mucosal cytotoxic $CD8^+$ T cells is associated with postoperative endoscopic recurrence in patients with Crohn's disease. J. Crohn's Colitis *10*, 338–345.

Brandhorst, S., Choi, I.Y., Wei, M., Cheng, C.W., Sedrakyan, S., Navarrete, G., Dubeau, L., Yap, L.P., Park, R., Vinciguerra, M., et al. (2015). A Periodic diet that mimics fasting promotes multi-system regeneration, enhanced cognitive performance, and healthspan. Cell Metab. *22*, 86–99.

Brockmann, L., Giannou, A.D., Gagliani, N., and Huber, S. (2017). Regulation of T_H17 cells and associated cytokines in wound healing, tissue regeneration, and carcinogenesis. Int. J. Mol. Sci. *18*, 1033.

Chassaing, B., Aitken, J.D., Malleshappa, M., and Vijay-Kumar, M. (2014). Dextran sulfate sodium (DSS)-induced colitis in mice. Curr. Protoc. Immunol. *104*, 15.25.

Cheng, C.-W., Adams, G.B., Perin, L., Wei, M., Zhou, X., Lam, B.S., Da Sacco, S., Mirisola, M., Quinn, D.I., Dorff, T.B., et al. (2014). Prolonged fasting reduces IGF-1/PKA to promote hematopoietic-stem-cell-based regeneration and reverse immunosuppression. Cell Stem Cell *14*, 810–823.

Cheng, C.-W., Villani, V., Buono, R., Wei, M., Kumar, S., Yilmaz, O.H., Cohen, P., Sneddon, J.B., Perin, L., and Longo, V.D. (2017). Fasting-mimicking diet promotes Ngn3-driven β-cell regeneration to reverse diabetes. Cell *168*, 775–788.e12.

Chiba, M., Tsuda, S., Komatsu, M., Tozawa, H., and Takayama, Y. (2016). Onset of ulcerative colitis during a low-carbohydrate weight-loss diet and treatment with a plant-based diet: a case report. Perm. J. *20*, 80–84.

Childers, R.E., Eluri, S., Vazquez, C., Weise, R.M., Bayless, T.M., and Hutfless, S. (2014). Family history of inflammatory bowel disease among patients with ulcerative colitis: a systematic review and meta-analysis. J. Crohn's Colitis *8*, 1480–1497.

Choi, I.Y., Piccio, L., Childress, P., Bollman, B., Ghosh, A., Brandhorst, S., Suarez, J., Michalsen, A., Cross, A.H., Morgan, T.E., et al. (2016). A diet mimicking fasting promotes regeneration and reduces autoimmunity and multiple sclerosis symptoms. Cell Rep. *15*, 2136–2146.

Choi, I.Y., Lee, C., and Longo, V.D. (2017). Nutrition and fasting mimicking diets in the prevention and treatment of autoimmune diseases and immunosenescence. Mol. Cell. Endocrinol. *455*, 4–12.

Ciorba, M.A., Riehl, T.E., Rao, M.S., Moon, C., Ee, X., Nava, G.M., Walker, M.R., Marinshaw, J.M., Stappenbeck, T.S., and Stenson, W.F. (2012). Lactobacillus probiotic protects intestinal epithelium from radiation injury in a TLR-2/cyclo-oxygenase-2-dependent manner. Gut *61*, 829–838.

Conn, P.M. (2013). Animal models for the study of human disease (Academic Press).

Couper, K.N., Blount, D.G., and Riley, E.M. (2008). IL-10: the master regulator of immunity to infection. J. Immunol. *180*, 5771–5777.

Damaskos, D., and Kolios, G. (2008). Probiotics and prebiotics in inflammatory bowel disease: microflora 'on the scope'. Br. J. Clin. Pharmacol. *65*, 453–467.

Dupaul-Chicoine, J., Yeretssian, G., Doiron, K., Bergstrom, K.S., McIntire, C.R., LeBlanc, P.M., Meunier, C., Turbide, C., Gros, P., Beauchemin, N., et al. (2010). Control of intestinal homeostasis, colitis, and colitis-associated colorectal cancer by the inflammatory caspases. Immunity *32*, 367–378.

Ellekilde, M., Selfjord, E., Larsen, C.S., Jakesevic, M., Rune, I., Tranberg, B., Vogensen, F.K., Nielsen, D.S., Bahl, M.I., Licht, T.R., et al. (2014). Transfer of gut microbiota from lean and obese mice to antibiotic-treated mice. Sci. Rep. *4*, 5922.

Eming, S.A., Wynn, T.A., and Martin, P. (2017). Inflammation and metabolism in tissue repair and regeneration. Science *356*, 1026–1030.

Everard, A., Lazarevic, V., Gaïa, N., Johansson, M., Ståhlman, M., Backhed, F., Delzenne, N.M., Schrenzel, J., François, P., and Cani, P.D. (2014). Microbiome of prebiotic-treated mice reveals novel targets involved in host response during obesity. ISME J. *8*, 2116–2130.

Ey, B., Eyking, A., Klepak, M., Salzman, N.H., Göthert, J.R., Rünzi, M., Schmid, K.W., Gerken, G., Podolsky, D.K., and Cario, E. (2013). Loss of TLR2 worsens spontaneous colitis in MDR1A deficiency through commensally induced pyroptosis. J. Immunol. *190*, 5676–5688.

Formeister, E.J., Sionas, A.L., Lorance, D.K., Barkley, C.L., Lee, G.H., and Magness, S.T. (2009). Distinct SOX9 levels differentially mark stem/progenitor populations and enteroendocrine cells of the small intestine epithelium. Am. J. Physiol. Gastrointest. Liver Physiol. *296*, G1108–G1118.

Freise, A.C., Zettlitz, K.A., Salazar, F.B., Tavaré, R., Tsai, W.K., Chatziioannou, A.F., Rozengurt, N., Braun, J., and Wu, A.M. (2018). ImmunoPET in inflammatory bowel disease: imaging CD4 T cells in a murine model of colitis. J. Nucl. Med. *59*, 980–985.

Funderburg, N.T., Stubblefield Park, S.R., Sung, H.C., Hardy, G., Clagett, B., Ignatz-Hoover, J., Harding, C.V., Fu, P., Katz, J.A., Lederman, M.M., and Levine, A.D. (2013). Circulating CD4(+) and CD8(+) T cells are activated in inflammatory bowel disease and are associated with plasma markers of inflammation. Immunology *140*, 87–97.

Gibson, G.R., Hutkins, R., Sanders, M.E., Prescott, S.L., Reimer, R.A., Salminen, S.J., Scott, K., Stanton, C., Swanson, K.S., Cani, P.D., et al. (2017). Expert consensus document: The International Scientific Association for Probiotics and Prebiotics (ISAPP) consensus statement on the definition and scope of prebiotics. Nat. Rev. Gastroenterol. Hepatol. *14*, 491–502.

Gupta, J., and Nebreda, A. (2014). Analysis of intestinal permeability in mice. Bio. Protoc *4*.

Henriksen, M., Jahnsen, J., Lygren, I., Stray, N., Sauar, J., Vatn, M.H., and Moum, B.; IBSEN Study Group (2008). C-reactive protein: a predictive factor and marker of inflammation in inflammatory bowel disease. Results from a prospective population-based study. Gut *57*, 1518–1523.

Hoffmann, M., Schwertassek, U., Seydel, A., Weber, K., Hauschildt, S., and Lehmann, J. (2017). Therapeutic efficacy of a combined sage and bitter apple phytopharmaceutical in chronic DSS-induced colitis. Sci. Rep. *7*, 14214.

Houchen, C.W., George, R.J., Sturmoski, M.A., and Cohn, S.M. (1999). FGF-2 enhances intestinal stem cell survival and its expression is induced after radiation injury. Am. J. Physiol. Gastrointest. Liver Physiol. *276*, 249–258.

Kaakoush, N.O. (2015). Insights into the Role of *Erysipelotrichaceae* in the Human Host. Front. Cell. Infect. Microbiol. *5*, 84.

Kaplan, G.G., and Ng, S.C. (2017). Understanding and preventing the global increase of inflammatory bowel disease. Gastroenterology *152*, 313–321.e2.

Karin, M., and Clevers, H. (2016). Reparative inflammation takes charge of tissue regeneration. Nature *529*, 307–315.

Kim, T.W., Seo, J.N., Suh, Y.H., Park, H.J., Kim, J.H., Kim, J.Y., and Oh, K.I. (2006). Involvement of lymphocytes in dextran sulfate sodium-induced experimental colitis. World J. Gastroenterol. *12*, 302–305.

Kim, J.J., Shajib, M.S., Manocha, M.M., and Khan, W.I. (2012). Investigating intestinal inflammation in DSS-induced model of IBD. J. Vis. Exp., 3678.

Koblansky, A.A., Truax, A.D., Liu, R., Montgomery, S.A., Ding, S., Wilson, J.E., Brickey, W.J., Mühlbauer, M., McFadden, R.M., Hu, P., et al. (2016). The innate immune receptor NLRX1 functions as a tumor suppressor by reducing colon tumorigenesis and key tumor-promoting signals. Cell Rep. *14*, 2562–2575.

Kuethe, J.W., Armocida, S.M., Midura, E.F., Rice, T.C., Hildeman, D.A., Healy, D.P., and Caldwell, C.C. (2016). Fecal microbiota transplant restores mucosal integrity in a murine model of burn injury. Shock *45*, 647–652.

Landy, J., Ronde, E., English, N., Clark, S.K., Hart, A.L., Knight, S.C., Ciclitira, P.J., and Al-Hassi, H.O. (2016). Tight junctions in inflammatory bowel diseases and inflammatory bowel disease associated colorectal cancer. World J. Gastroenterol. *22*, 3117–3126.

Larmonier, C.B., Shehab, K.W., Ghishan, F.K., and Kiela, P.R. (2015). T lymphocyte dynamics in inflammatory bowel diseases: role of the microbiome. Biomed. Res. Int., *2015*, 504638.

Lee, C., and Longo, V. (2016). Dietary restriction with and without caloric restriction for healthy aging. F1000Research, *5*, F1000 Faculty Rev–117.

Leppkes, M., Roulis, M., Neurath, M.F., Kollias, G., and Becker, C. (2014). Pleiotropic functions of TNF-α in the regulation of the intestinal epithelial response to inflammation. Int. Immunol. *26*, 509–515.

Lichtenstein, G.R. (2013). Comprehensive review: antitumor necrosis factor agents in inflammatory bowel disease and factors implicated in treatment response. Therap. Adv. Gastroenterol. *6*, 269–293.

Loudhaief, R., and Gallet, A. (2016). Enteroendocrine cells, a potential way to control intestinal stem cell proliferation. Int. J. Stem Cell Res. Ther. *3*, 037.

Manichanh, C., Borruel, N., Casellas, F., and Guarner, F. (2012). The gut microbiota in IBD. Nat. Rev. Gastroenterol. Hepatol. *9*, 599–608.

Markowiak, P., and Śliżewska, K. (2017). Effects of probiotics, prebiotics, and synbiotics on human health. Nutrients *9*, 1021.

Mayer, J.U., Demiri, M., Agace, W.W., Macdonald, A.S., Svensson-Frej, M., and Milling, S.W. (2017). Different populations of CD11b dendritic cells drive Th2 responses in the small intestine and colon. Nat. Commun *8*, 15820.

Michielan, A., and D'Incà, R. (2015). Intestinal permeability in inflammatory bowel disease: pathogenesis, clinical evaluation, and therapy of leaky gut. Mediators of Inflammation *2015*, 628157.

Mihaylova, M.M., Cheng, C.W., Cao, A.Q., Tripathi, S., Mana, M.D., Bauer-Rowe, K.E., Abu-Remaileh, M., Clavain, L., Erdemir, A., Lewis, C.A., et al. (2018). Fasting activates fatty acid oxidation to enhance intestinal stem cell function during homeostasis and aging. Cell Stem Cell *22*, 769–778.e4.

Morgan, M.E., Zheng, B., Koelink, P.J., van de Kant, H.J., Haazen, L.C., van Roest, M., Garssen, J., Folkerts, G., and Kraneveld, A.D. (2013). New perspective on dextran sodium sulfate colitis: antigen-specific T cell development during intestinal inflammation. PLoS ONE *8*, e69936.

Neurath, M.F. (2014). Cytokines in inflammatory bowel disease. Nat. Rev. Immunol. *14*, 329–342.

Okada, T., Otsubo, T., Hagiwara, T., Inazuka, F., Kobayashi, E., Fukuda, S., Inoue, T., Higuchi, K., Kawamura, Y.I., and Dohi, T. (2017). Intermittent fasting prompted recovery from dextran sulfate sodium-induced colitis in mice. J. Clin. Biochem. Nutr. *61*, 100–107.

Olsen, T., Rismo, R., Cui, G., Goll, R., Christiansen, I., and Florholmen, J. (2011). T_H1 and T_H17 interactions in untreated inflamed mucosa of inflammatory bowel disease, and their potential to mediate the inflammation. Cytokine *56*, 633–640.

Raza, G.S., Putaala, H., Hibberd, A.A., Alhoniemi, E., Tiihonen, K., Mäkelä, K.A., and Herzig, K.H. (2017). Polydextrose changes the gut microbiome and attenuates fasting triglyceride and cholesterol levels in Western diet fed mice. Sci. Rep. *7*, 5294.

Reunanen, J., Kainulainen, V., Huuskonen, L., Ottman, N., Belzer, C., Huhtinen, H., de Vos, W.M., and Satokari, R. (2015). Akkermansia muciniphila adheres to enterocytes and strengthens the integrity of the epithelial cell layer. Appl. Environ. Microbiol. *81*, 3655–3662.

Rose, W.A., 2nd, Sakamoto, K., and Leifer, C.A. (2012). TLR9 is important for protection against intestinal damage and for intestinal repair. Sci. Rep. *2*, 574.

Roy, U., Gálvez, E.J.C., Iljazovic, A., Lesker, T.R., Błażejewski, A.J., Pils, M.C., Heise, U., Huber, S., Flavell, R.A., and Strowig, T. (2017). Distinct microbial communities trigger colitis development upon intestinal barrier damage via innate or adaptive immune cells. Cell Rep. *21*, 994–1008.

Russell, W.R., Gratz, S.W., Duncan, S.H., Holtrop, G., Ince, J., Scobbie, L., Duncan, G., Johnstone, A.M., Lobley, G.E., Wallace, R.J., et al. (2011). High-protein, reduced-carbohydrate weight-loss diets promote metabolite profiles likely to be detrimental to colonic health. Am. J. Clin. Nutr. *93*, 1062–1072.

Sartor, R.B. (2006). Mechanisms of disease: pathogenesis of Crohn's disease and ulcerative colitis. Nat. Clin. Pract. Gastroenterol. Hepatol. *3*, 390–407.

Sato, T., van Es, J.H., Snippert, H.J., Stange, D.E., Vries, R.G., van den Born, M., Barker, N., Shroyer, N.F., van de Wetering, M., and Clevers, H. (2011). Paneth cells constitute the niche for Lgr5 stem cells in intestinal crypts. Nature *469*, 415–418.

Sävendahl, L., Underwood, L.E., Haldeman, K.M., Ulshen, M.H., and Lund, P.K. (1997). Fasting prevents experimental murine colitis produced by dextran sulfate sodium and decreases interleukin-1 β and insulin-like growth factor I messenger ribonucleic acid. Endocrinology *138*, 734–740.

Schippers, A., Muschaweck, M., Clahsen, T., Tautorat, S., Grieb, L., Tenbrock, K., Gaßler, N., and Wagner, N. (2016). β7-Integrin exacerbates experimental DSS-induced colitis in mice by directing inflammatory monocytes into the colon. Mucosal Immunol. *9*, 527–538.

Seedorf, H., Griffin, N.W., Ridaura, V.K., Reyes, A., Cheng, J., Rey, F.E., Smith, M.I., Simon, G.M., Scheffrahn, R.H., Woebken, D., et al. (2014). Bacteria from diverse habitats colonize and compete in the mouse gut. Cell *159*, 253–266.

Shatzkes, K., Tang, C., Singleton, E., Shukla, S., Zuena, M., Gupta, S., Dharani, S., Rinaggio, J., Connell, N.D., and Kadouri, D.E. (2017). Effect of predatory bacteria on the gut bacterial microbiota in rats. Sci. Rep. *7*, 43483.

Srutkova, D., Schwarzer, M., Hudcovic, T., Zakostelska, Z., Drab, V., Spanova, A., Rittich, B., Kozakova, H., and Schabussova, I. (2015). Bifidobacterium longum CCM 7952 promotes epithelial barrier function and prevents acute DSS-induced colitis in strictly strain-specific manner. PLoS One *10*, e0134050.

Sun, H., Lou, Y., Porturas, T., Morrissey, S., Luo, G., Qi, J., Ruan, Q., Shi, S., and Chen, Y.H. (2015). Exacerbated experimental colitis in TNFAIP8-deficient mice. J. Immunol. *194*, 5736–5742.

Tinkum, K.L., Stemler, K.M., White, L.S., Loza, A.J., Jeter-Jones, S., Michalski, B.M., Kuzmicki, C., Pless, R., Stappenbeck, T.S., Piwnica-Worms, D., et al. (2015). Fasting protects mice from lethal DNA damage by promoting small intestinal epithelial stem cell survival. Proc. Natl. Acad. Sci. U S A *112*, 148–154.

Van Landeghem, L., Blue, R.E., Dehmer, J.J., Henning, S.J., Helmrath, M.A., and Lund, P.K. (2012). Localized intestinal radiation and liquid diet enhance survival and permit evaluation of long-term intestinal responses to high dose radiation in mice. PLoS One *7*, e51310.

Vermeire, S., Van Assche, G., and Rutgeerts, P. (2006). Laboratory markers in IBD: useful, magic, or unnecessary toys? Gut *55*, 426–431.

Wei, M., Brandhorst, S., Shelehchi, M., Mirzaei, H., Cheng, C.W., Budniak, J., Groshen, S., Mack, W.J.E., Guen, E., Di Biase, S., et al. (2017). Fasting-mimicking diet and markers/risk factors for aging, diabetes, cancer, and cardiovascular disease. Sci. Transl. Med. *9*, eaai8700.

Whibley, N., and Gaffen, S.L. (2015). Gut-busters–IL-17 ain't afraid of no IL-23. Immunity, *43*(4), 620–622. Wirtz, S., Popp, V., Kindermann, M., Gerlach, K., Weigmann, B., Fichtner-Feigl, S., Neurath, M.F. (2017). Chemically induced mouse models of acute and chronic intestinal inflammation. Nat. Protoc. *12*, 1295–1309.

Wirtz, S., Popp, V., Kindermann, M., Gerlach, K., Weigmann, B., Fichtner-Feigl, S., and Neurath, M.F. (2017). Chemically induced mouse models of acute and chronic intestinal inflammation. Nat. Protoc *12*, 1295–1309.

Yan, Y., Laroui, H., Ingersoll, S.A., Ayyadurai, S., Charania, M., Yang, S., Dalmasso, G., Obertone, T.S., Nguyen, H., Sitaraman, S.V., and Merlin, D. (2011). Overexpression of Ste20-related proline/alanine-rich kinase exacerbates experimental colitis in mice. J. Immunol. *187*, 1496–1505.

Yilmaz, Ö.H., Katajisto, P., Lamming, D.W., Gültekin, Y., Bauer-Rowe, K.E., Sengupta, S., Birsoy, K., Dursun, A., Yilmaz, V.O., Selig, M., et al. (2012). mTORC1 in the Paneth cell niche couples intestinal stem-cell function to calorie intake. Nature *486*, 490–495.

Zhang, Y.Z., and Li, Y.Y. (2014). Inflammatory bowel disease: pathogenesis. World J. Gastroenterol. *20*, 91–99.

Zou, Y., Lin, J., Li, W., Wu, Z., He, Z., Huang, G., Wang, J., Ye, C., Cheng, X., Ding, C., et al. (2016). Huangqin-tang ameliorates dextran sodium sulphate-induced colitis by regulating intestinal epithelial cell homeostasis, inflammation and immune response. Sci. Rep. *6*, 39299.

STAR★METHODS

KEY RESOURCES TABLE

REAGENT or RESOURCE	SOURCE	IDENTIFIER
Antibodies		
mouse anti-CD4 (1:200; IHC)	eBioscience from Thermo Fisher Scientific	Cat#14-0041-86; RRID: AB_467063
rat anti-CD8 (1:200; IHC)	Abcam	Cat#ab22378; RRID: AB_447033
rabbit anti-Lgr5 (1:200; IHC)	Abcam	Cat#ab75732; RRID: AB_1310281
mouse anti-Sox9 (1μg/ml; IHC).	eBioscience from Thermo Fisher Scientific	Cat#14-9765-80; RRID: AB_2573005
Alexafluor 488 anti-mouse/human CD11b (1:200; IHC)	BioLegend	Cat#101219; RRID: AB_493545
donkey anti-rabbit Alexafluor 594 (1:300; IHC),	Thermo Fisher Scientific	Cat#A21207; RRID: AB_141637
donkey anti-mouse Alexafluor 488 (1:300; IHC)	Thermo Fisher Scientific	Cat#A21202; RRID: AB_141607
donkey anti-rat Alexafluor 594 (1:300; IHC)	Thermo Fisher Scientific	Cat#A21209; RRID: AB_2535795
CD3 Alexa700 (0.25 μg/test; FACS)	eBioscience from Thermo Fisher Scientific	Cat#56-0032-82; RRID: AB_529507
CD4 PE-Cy5 (0.06 μg/test; FACS)	eBioscience from Thermo Fisher Scientific	Cat#15-0041-82; RRID: AB_468695
CD8 Alexa488 (0.5 μg/test; FACS)	eBioscience from Thermo Fisher Scientific	Cat#53-0081-82; RRID: AB_469897
CD44 APC (0.06 μg/test; FACS)	eBioscience from Thermo Fisher Scientific	Cat#17-0441-82; RRID: AB_469390
CD62L PE-Cy7 (0.25 μg/test; FACS)	eBioscience from Thermo Fisher Scientific	Cat#25-0621-82; RRID: AB_469633
CD19 PE (0.125 μg/test; FACS)	eBioscience from Thermo Fisher Scientific	Cat#12-0193-82; RRID: AB_657661
CD11b PE-eFluor 610 (0.25 μg/test; FACS)	eBioscience from Thermo Fisher Scientific	Cat#61-0112-82; RRID: AB_2574528
F4/80 PE-Cy5 (0.25 μg/test; FACS)	eBioscience from Thermo Fisher Scientific	Cat#15-4801-82; RRID: AB_468798
Ly-6G(ar-1) APC (0.5 μg/test; FACS)	eBioscience from Thermo Fisher Scientific	Cat#17-9668-82; RRID: AB_2573307
CD45 APC-eFluor 780 (0.125 μg/test; FACS)	eBioscience from Thermo Fisher Scientific	Cat#47-0451-82; RRID: AB_1548781
Bacterial and Virus Strains		
Lactobacillus rhamnosus GG (LGG)	ATCC	ATCC 53103
Biological Samples		
Human serum	Clinical Trial	NCT02158897
Chemicals, Peptides, and Recombinant Proteins		
Dextran sulfate sodium salt (DSS)	Alfa Aesar by Thermo Fisher Scientific	Cat#J14489-22; CAS:9011-18-1
Paraformaldehyde	Sigma-Aldrich	Cat#158127; CAS:30525-89-4
5-Bromo-2′-deoxyuridine (BrdU)	Sigma-Aldrich	Cat#B002; CAS:59-14-3
Normal Donkey Serum	Jackson ImmunoResearch	Cat#017-000-121
Polyvinyl alcohol mounting medium with DABCO, antifading	Sigma-Aldrich	Cat#10981
Fluorescein isothiocyanate–dextran	Sigma-Aldrich	Cat# FD4; CAS: 60842-46-8
Hoechst 33342 Solution	Thermo Fisher Scientific	Cat#62249
Critical Commercial Assays		
Hematoxylin & Eosin Stain Kit	Vector Laboratories	Cat#H-3502
BrdU *In Situ* Detection Kit	BD Biosciences	Cat#550803
Mouse TNF-alpha Quantikine ELISA Kit	R&D Systems	Cat#MTA00B
Mouse IFN-gamma Quantikine ELISA Kit	R&D Systems	Cat#MIF00
Mouse IL-17 Quantikine ELISA Kit	R&D Systems	Cat#M1700
ProcartaPlex Custom Multiplex Panel	Thermo Fisher Scientific	Cat#PPX-11; Design ID: MX9HH77
Experimental Models: Organisms/Strains		
Mouse: C57BL/6J	The Jackson Laboratory	JAX: 000664
Software and Algorithms		
ImageJ	NIH	https://imagej.nih.gov/ij/
GraphPad Prism v.7	Graphpad	https://www.graphpad.com/

(*Continued on next page*)

Continued

REAGENT or RESOURCE	SOURCE	IDENTIFIER
cellSens Standard	Olympus	https://www.olympus-lifescience.com/en/software/cellsens/
BD FACSDiva	BD Biosciences	http://www.bdbiosciences.com/us/instruments/research/software/flow-cytometry-acquisition/bd-facsdiva-software/m/111112/overview
FloJo Software	BD Biosciences	https://www.flowjo.com/solutions/flowjo/downloads
Other		
Mouse diet: Fasting mimicking diet (FMD)	Cheng et al., 2017	N/A
Human diet: Fasting mimicking diet (FMD)	Propriety formulation belonging to L-Nutra	http://www.l-nutra.com/prolon/
Control Diet: PicoLab Rodent Diet 20	LabDiet	Cat#5053
Irradiated Sterile Diet: Pico-Vac Lab Rodent Diet	LabDiet	Cat#5061
HydroGel	ClearH_2O	N/A
Hemoccult II SENSA Fecal Occult Blood Test Systems	Beckman Coulter	Cat# 10012-018
Hemavet 950 System	Drew Scientific	N/A
Bead Ruptor 12	Omni International	Cat#19-050A
CO_2 pouch system	BD Diagnostics	Cat#260684/ 90003-650
Lactobacilli MRS Agar	BD Diagnostics	Cat#288210
Lactobacilli MRS Broth	BD Diagnostics	Cat#288130
Microbiome sequencing: V4 16S rRNA gene sequencing (Illumina MiSeq platform)	Second Genome Solutions; South San Francisco, CA, USA	N/A
EVOS FL Imaging System	Thermo Fisher Scientific	Cat# AMF4300
All-in-One Fluorescence Microscope	Keyence	Cat# BZ-X710
Olympus BX50 Microscope	Olympus	N/A
Olympus DP73 Camera	Olympus	N/A
BD LSR II	BD Biosciences	N/A
Bio-Plex Suspension Array System	BioRad	N/A
SpectraMax M2 Microplate Reader	Molecular Devices	N/A

CONTACT FOR REAGENT AND RESOURCE SHARING

Further information and requests for reagents may be directed to and will be fulfilled by the Lead Contact, Valter D. Longo (vlongo@usc.edu).

EXPERIMENTAL MODEL AND SUBJECT DETAILS

Mouse Models

All animal protocols were approved by the Institutional Animal Care and Use Committee (IACUC) of the University of Southern California (USC). All mice were maintained in a pathogen-free environment and housed in clear shoebox cages in groups of five animals per cage with constant temperature and humidity and 12 hr/12 hr light/dark cycle. Prior to supplying the FMD diet, animals were transferred into fresh cages to avoid feeding on residual chow and coprophagy. All animals had access to water at all times. Unless otherwise on experimental diets, mice were fed *ad libitum* with regular chow (e.g., PicoLab Rodent Diet 20).

Chronic dextran sodium sulfate (DSS)-induced mouse model

C57BL/6 mice (8-weeks-old, female) were purchased from The Jackson Laboratory and group-housed for 33 days. Before starting DSS administration, mice were randomly-assigned into a Naive or DSS group. All mice were fed a ground standard rodent chow (PicoLab Rodent Diet 20, LabDiet) and the DSS group received water with 2% w/w Dextran sulfate sodium salt (DSS, Alfa Aesar) mixed into autoclaved water as the only drinking source for 5 consecutive days, followed by 9 consecutive days of purified water. This defined one DSS cycle. After 33 days, mice were randomly-assigned to experimental groups and single-housed for the remainder of the experiment, encompassing part of the 3rd DSS cycle (9 consecutive days of purified water) and 4th DSS cycle. Mice either underwent two, 2-day water-only fasting cycles, or two, 4-day cycles of FMD during this time frame. On the first day

of each water-only fasting or FMD cycle, animals were transferred into fresh cages to avoid feeding on residual chow and coprophagy. Mice were immediately refed with ground standard rodent chow (PicoLab Rodent Diet 20, LabDiet) after 2 days (water-only fast) or 4 days (FMD) of the diet cycles. Individual body weights and food consumption was measured daily for the entire duration of the study.

Fecal transplant and Lactobacillus transplant models

The fecal transplant was performed in mice based on previously published protocols (Seedorf et al., 2014; Ellekilde et al., 2014; Kuethe et al., 2016; Shatzkes et al., 2017). Briefly, ceca contents were removed from naive and chronic DSS-induced mice (with or without FMD treatment) and were aseptically flushed into a sterile 50% glycerol/PBS solution, in a 1:10 dilution. The mixed ceca solutions were then aliquoted and frozen at −80°C until time of use. On each day of inoculation, the aliquots from the pooled cecum solutions specific for each group were diluted again, 1:5, and administered at a volume of 150μL per mouse. The Lactobacillus transplant in DSS-treated mice was performed based on previous protocols (Ciorba et al., 2012), in lieu of a fecal transplant. Briefly, Lactobacillus rhamnosus GG (LGG) (ATCC 53103) was purchased from American Tissue Culture Collection (ATCC, Manassas, Virginia, USA) and cultured according to manufacturer's instructions, in Lactobacilli MRS broth (BD Diagnostics, 288130) at 37°C for 48 hours. Petri dishes containing Lactobacilli MRS Agar (BD Diagnostics, 288210) were used to confirm the concentrations of live bacteria by serial dilutions. These plates were sealed in a CO2 pouch system (BD Diagnostics, 260684) and placed in an incubator at 37°C for 48 hours. Aliquots containing of 5x107 cfu/mouse/day were suspended in 50% PBS-glycerol solution and frozen at −80°C in cryovials until day of gavage. C57BL/6 mice (8-weeks-old, female) were purchased from The Jackson Laboratory, group-housed for 33 days, and were on a food and water schedule to initiate the DSS condition previously described in the above section. After 33 days, mice were single-housed for the remainder of the experiment and were only allowed to consume an irradiated sterile diet (Pico-Vac Lab Rodent Diet, LabDiet) and autoclaved water. Mice were orally-gavaged 3 days after being single-housed, for 4 consecutive days to match the duration of an FMD cycle. Mice were divided into three groups: one receiving the pooled ceca solution from donor mice that underwent four DSS cycles and no dietary intervention (DSS Fecal Transplant (FT)), the second receiving the pooled ceca solution from donor mice that underwent four DSS cycles and two FMD cycles (DSS+FMD FT), and a group receiving the Lactobacillus transplant (DSS+LGG). A Naive control group received no DSS, but a 1:1 control gavage solution of sterile 50% glycerol/PBS (Naive FT). Mice were euthanized one week after the last day of inoculation.

Human FMD trial

All participants provided written informed consent, and the University of Southern California (USC) Institutional Review Board approved the protocol (approval #HS-12-00391). The design, dietary composition, and results of the human FMD trial have been reported elsewhere (Wei et al., 2017). In brief, one-hundred participants (generally healthy adult volunteers and 18 to 70 years of age; BMI, 18.5 and up) without a diagnosed medical condition in the previous 6 months were enrolled (ClinicalTrials.gov: NCT02158897). All data was collected at the USC Diabetes and Obesity Research Institute; subjects were recruited from April 2013 to July 2015. Participants were instructed to consume the FMD, which was provided in a box, for 5 continuous days, and to return to their normal diet after completion until the next cycle that was initiated approximately 25 days later. Participants completed three cycles of this 5-day FMD. Participants completed baseline (A) and follow-up examinations at the end of the first FMD (before resuming normal diet to measure the acute FMD effects; B) and after a washout period of 5 to 7 days of normal caloric intake after the third FMD cycle (C). A complete blood count was performed at each time point by an overnight fasting blood draw through venipuncture at the USC Diabetes and Obesity Research Institute. WBC and lymphocyte data was stratified post hoc for all subjects that successfully completed 3 FMD cycles with C-reactive protein levels lower than 1 mg/L (normal risk group) versus subjects with > 1 mg/L CRP (elevated risk group) at baseline.

Criteria for inclusion of human subjects

Generally healthy adult volunteers, subjects 18-70 years of age, body mass index, 18.5 and up, ability and willingness to provide written informed consent, ability, and willingness to undergo multiple cycles of a 5-day dietary regimen, ability and willingness to provide blood samples via venipuncture.

Exclusion criteria

Any major medical condition or chronic diseases, mental illness, drug dependency, hormone replacement therapy (dehydroepiandrosterone, estrogen, thyroid, and testosterone), pregnant or nursing female, special dietary requirements or food allergies, alcohol dependency, and medications known to affect body weight.

Profile

Subjects in this study are at age 43.0 ± 11.2 years, with heights of 168.3 ± 9.8 cm, with body weights of 77.7 ± 16.8 kg at baseline and 75.5 ± 16.4 kg at the end of FMD. The female:male distribution is as follows: low CRP (N = 36; 15:21) and high CRP with FMD (N = 25; 16:9).

METHOD DETAILS

Mouse fasting mimicking diet

The mouse version of the FMD is a 4-day regimen based on the human FMD (Wei et al., 2017; Brandhorst et al., 2015) and has been previously detailed (Cheng et al., 2017). Briefly, a combination of flavored broth mixes, extra virgin olive oil (EVOO), essential fatty acids, vegetable powders (containing beet root, carrot root, collard leaf, kale leaf, nettle leaf, spinach leaf, tomato fruit, and mitake mushroom), vitamins, and minerals were thoroughly mixed and bound together with heated hydrogel (ClearH_20, Maine) on Day 1 of the diet. From Days 2-4, a combination of flavored broth mixes, glycerol, and hydrogel was fed to mice. On the first day of FMD, mice consumed ≈50% of their normal caloric intake (8.08 kJ/g; 0.56 kJ fat, 0.68 kJ carbohydrates, 0.11 kJ protein). From the second through fourth days of FMD, mice consumed ≈10% of their normal caloric intake (1.10 kJ/g; 0.27 kJ carbohydrates). All mice were supplied with fresh food during the morning hours (9am-11am), with most of the food consumed within the first few hours of the light cycle. Control-fed animals normally consumed food within the dark hours.

Post-diet refeeding

After the end of each 2-day water-only fast and 4-day FMD cycle, mice were fed *ad libitum* with regular chow (PicoLab Rodent Diet 20, LabDiet) to regain body weight before the next diet cycle.

DAI scoring

DAI is used to track the severity of the disease by scoring the extent of body weight loss, stool consistency, and blood in the stools (Kim et al., 2012).The DAI for each animal was recorded once after every 5-day DSS administration period for the first two DSS cycles, and then every day starting after the third DSS cycle. Scores were determined based on body weight loss, stool consistency, and rectal bleeding as described previously (Sun et al., 2015). Body weight loss was scored as follows: score 0, no body weight loss; score 1, body weight loss within 1%–5%; score 2, body weight loss within 5%–10%; score 3, body weight loss within 10%–20%; score 4, greater than 20% body weight loss. Stool consistency was determined as follows: score 0, solid pellets; score 1, soft but adherent in pellet shape; score 2, loose stool but with some solidity; score 3, loose stool with signs of liquid consistency; score 4, diarrhea. Rectal bleeding was evaluated using a Hemoccult II SENSA Fecal Occult Blood Test Kit (Beckman Coulter) and following the manufacturer's protocol. Scoring was determined as follows: score 0, no sign of blood; score 1, Hemoccult positive; score 2, Hemoccult positive with visual pellet bleeding; score 3, Hemoccult positive with visual pellet and rectal bleeding; score 4, Hemoccult positive with gross visual pellet and rectal bleeding. The total sum from stool consistency and rectal bleeding was recorded as the overall DAI score, since temporary body weight loss from the water-only fasting and/or FMD cycles could interfere with accurate disease severity, as it reflects accurate reduction of caloric intake, and not reduced health (Brandhorst et al., 2015).

Colon inflammation score

H&E stained proximal colon sections were analyzed for severity of colonic inflammation 9 days after the 4^{th} DSS cycle (DSS) and 9 days after the 4^{th} DSS cycle and 5 days after the last FMD cycle (DSS+FMD), as defined by the abundance of acute and inflammatory infiltrates such as lymphocytes, macrophages, and neutrophils, spanning the mucosa, *muscularis mucosae*, and submucosa. A basal level of inflammation was scored at 0 (the Naive group was used as a control), a slight increase over the normal level of inflammatory cells was scored as mild (1), a more obvious increase was scored as moderate (2), with a significantly higher increase from basal inflammation scored as severe (3), all of which was tabulated into a numerical score.

BrdU Injection

BrdU (Sigma-Aldrich) was prepared in heated and intra-peritoneal (i.p.) injected into mice 24 hours before euthanasia (1mg/100ul/mouse). A second and final BrdU injection was given 4 hours before euthanasia (1mg/100ul/mouse). Mice were fasted for 4 hours prior to second and final BrdU injection.

Immunohistochemistry analysis

On the 3^{rd} day after the last FMD cycle was completed, mice were euthanized, and serum, spleen, small intestine, and big intestine (ceca and colon) tissue was collected. Serum and spleens were kept on ice for FACS-processing and cytokine measurements. Big intestines were straightened to measure colon length, and ceca contents were removed for the fecal transplant experiment. Small and big intestinal tissue was then cut and either flash-frozen and stored at −80°C or fixed in 4% PFA and further processed in a sucrose gradient, OCT-embedded, sectioned, and stained. The jejunum portion of the small intestine and the proximal colon of the big intestine were used for all staining procedures described here, and the tissue preparation described has been adapted from previous protocols (Van Landeghem et al., 2012; Ey et al., 2013). Intestinal tissue was fixed in 4% PFA overnight, rinsed in 1X PBS and suspended in a 10% sucrose solution overnight. To complete the cryoprotection process, tissues were finally suspended in a 30% sucrose solution overnight. Tissues were then embedded in optical cutting temperature medium (OCT), flash-frozen on dry ice, and stored at −80°C until ready for cryo-sectioning. Sections were transversally cut at 7μm and adhered to positively-charged microscope slides. The exception to this procedure was for H&E staining: proximal colon sections were not fixed in 4% PFA and were immediately kept in 1X PBS after cutting open longitudinally, rolled with a toothpick, mounted in cryomolds using OCT, and

flash-frozen on dry ice. Sections were transversally cut at 4μm and adhered to positively-charged slides that were stained with the Hematoxylin & Eosin Stain Kit (Vector Laboratories, H-3502) following the manufacturer's protocol to visualize general changes in epithelial and crypt morphology. To quantify colonic crypt number for each animal, representative images from each section (3-4) of a slide were taken, and the distance in pixels was measured along the muscularis mucosae. The distance was converted to μm, and the number of crypts counted over the measured distance was normalized to a number over 5000 μm. For immunofluorescent staining of CD4, CD8, CD11b, Lgr5, Sox9, and BrdU, slides containing jejunum small intestine and proximal colon sections were thawed at room temperature, rehydrated with PBS, blocked for non-specific staining in blocking buffer (1% Normal Donkey Serum in PBS, Jackson ImmunoResearch) for 30 min at room temperature, and stained with primary antibodies overnight at 4°C. The next day, the sections were washed and stained with secondary antibodies for 1 hour at room temperature. Sections were protected from light, washed in PBS, stained with Hoechst 33342 (Thermo Fisher) to stain for nuclei, and coverslipped with anti-fading polyvinyl alcohol mounting medium with DABCO (Sigma-Aldrich). Images were captured at 20X using the EVOS FL Cell Imaging System (Thermo Fisher) and BZ-X710 All-in-One Fluorescence Microscope (Keyence) and analyzed with ImageJ (National Institute of Health). The quantification of CD4, CD8 and Sox9 positive cells was limited to the villi region for small intestine sections, and the number of positive cells in 30-50 villi per animal were counted (at least 50 for Sox9). The quantification of Lgr5 was localized to the crypt region for both the small intestine and colon samples, and the number of positive cells in 50 crypts per animal were counted. The quantification of CD4, CD8, and Cd11b for colon sections was limited to the LP surrounding the base of colonic crypts. The area surrounding 50 randomized crypts per animal were counted. The average number of positive cells per villi or crypt was then derived from these calculations. For BrdU positive cell detection in the crypts of small intestine jejunum and proximal colon tissue, sections were stained with BrdU *In Situ* Detection Kit (BD Biosciences, 550803) following the manufacturer's 3,3′-diaminobenzidine (DAB)-based protocol. Images were observed with an Olympus BX50 microscope and Olympus DP73 camera and captured at 20X (colon) or 40X (small intestine) magnification with cellSens Standard (Olympus Corp.) software. The number of positive BrdU cells in 50 crypts per animal was counted, starting from the base of the crypt to two-thirds of the way up from the base. The average number of BrdU positive cells per crypt was then derived from these calculations. Primary antibodies used for small intestine and colon immunofluorescent staining: mouse anti-CD4 (eBioscience, 14-0041-86), rat anti-CD8 (Abcam, ab22378), rabbit anti-Lgr5 (Abcam, ab75732, 1:200), mouse anti-Sox9 (eBioscience, 14-9765-80). Secondary and secondary-conjugated primary antibodies used for small intestine and colon immunofluorescent staining: Alexafluor 488 anti-mouse/human CD11b (BioLegend, 101219), donkey anti-rabbit Alexafluor 594 (Thermo Fisher, A21207), donkey anti-mouse Alexafluor 488 (Thermo Fisher, A21202), and donkey anti-rat Alexafluor 594 (ThermoFisher, A21209).

FACS Analysis

FACS analyses for different immune cell populations were conducted following standard protocols. Freshly-harvested splenocytes and peripheral blood mononuclear cells (PBMCs) were stained with the immune cell markers listed below and analyzed with BD FACS Diva on LSR II. Antibodies used for FACS analysis: CD3 Alexa700 (eBioscience), CD4 PE-Cy5 (eBioscience), CD8 Alexa488 (eBioscience), CD44 APC (eBioscience), CD62L PE-Cy7 (eBioscience), CD19 PE (eBioscience), CD11b Pe-eFluor 610 (eBioscience), F4/80 PE-Cy5 (eBioscience), Ly-6G(ar-1) APC (eBioscience), CD45 APC-eFluor 780 (eBioscience).

Cytokines profiling

Prior to blood collection, mice were fasted for eight hours. Serum was stored at −80°C. Complete blood counts were executed with the Hemavet 950 System (Drew Scientific) following the manufacturer's protocol in order to evaluate whole-blood parameters. Proximal colon pieces (approximately 2 cm from the bottom of cecum) were cut longitudinally and cultured individually in 6-well plates at 37°C in a cell culture room incubator in RPMI 1640 medium with 1% antibiotic. After 24 hours, the medium for each sample was centrifuged at 800 g for 20 minutes, and the resulting supernatant was kept at −20°C until time of use. Distal colon tissue was weighed and homogenized with the Bead Ruptor 12 (Omni International) according to standard protocols. After centrifugation and purification, the resulting tissue homogenate was kept at −80°C until time of use. TNF-α, IFN-γ, and IL-17A (R&D Systems) were measured following the manufacturer's protocol and using a spectrophotometer (SpectraMax M2, Molecular Devices). Serum, colonic supernatant, and colonic tissue homogenate levels of IFN-γ, IL-13, IL-23, IL-17A, IL-10, IL-27, IL-5, IL-6, and TNF-α for the Naive FT, DSS FT, and DSS+FMD FT groups were measured on a custom ProcartaPlex Multiplex Panel (Thermo Fisher), with the plate read by a BioRad Bio-Plex Suspension Array System (BioRad).

FITC Dextran Permeability

Increased gut permeability was evaluated by an increase in the serum concentration of fluorescein isothiocyanate conjugated dextran (FITC-Dextran). Based on previously published methods (Yan et al., 2011; Gupta and Nebreda, 2014; Michielan and D'Incà, 2015), mice were fasted for four hours prior to oral gavage with 60mg/100 g of fluorescein isothiocyanate conjugated dextran (FITC-dextran, Sigma-Aldrich). At the time of euthanasia, four hours after the gavage, serum was collected through cardiac puncture and shielded from light on ice. Samples were plated on a 96-well plate at a 1:2 dilution with PBS, with concentrations read using a spectrophotometer (SpectraMax M2, Molecular Devices). Serum from mice that did not undergo FITC-dextran gavage was used to create a standard curve.

Microbiome sequencing

Fecal stool samples from the experimental groups were shipped to Second Genome Solutions (South San Francisco, CA, USA) for V4 16S rRNA gene sequencing using an Illumina MiSeq platform and a microbial profiling report summarizing the results was provided.

Human fasting-mimicking diet

The human version of the FMD in a proprietary formulation belonging to L-Nutra (http://www.l-nutra.com/prolon/). It is a plant-based diet designed to attain fasting-like effects on the serum levels of IGF-1, IGFP1, glucose and ketone bodies while providing both macronutrients and micronutrients to minimize the burden of fasting (Brandhorst et al., 2015). Day 1 of the FMD supplies ~4600 kJ (11% protein, 46% fat, 43% carbohydrate), whereas days −5 provide ~3000 kJ (9% protein, 44% fat, 47% carbohydrate) per day. The FMD is comprised of proprietary formulations of vegetable-based soups, energy bars, energy drinks, chip snacks, tea, and a supplement containing minerals, vitamins, and essential fatty acids. All items to be consumed per day were individually boxed to allow the subjects to choose when to eat while avoiding accidentally consuming components of the following day. A suggested meal plan was provided that described when the study foods could be consumed (i.e., breakfast, lunch, snacks, and dinner). The ingredients of the diet have been detailed previously (Wei et al., 2017), and are outlined below:

Ingredients

Vegetable Soup: Rice Flour, Dried Onion, Inulin (Chicory Fiber), Dried Tomato, Dried Carrot, Salt, Dried Red Pepper, Dried Leek, Potato Starch, Olive Oil, Freeze-dried Basil, Spinach Powder, Dried Parsley, Natural Flavor.

Mushroom Soup: Rice Flour, Carrot Powder, Dried Onion, Champignon Mushroom Powder, Inulin (Chicory Fiber), Dried Champignon Mushroom, Salt, Yeast Extract, Potato Starch, Olive Oil, Dried Parsley, Natural Flavor.

Tomato Soup: Rice Flour, Dried Tomato Powder, Dried Onion, Inulin (Chicory Fiber), Potato Starch, Dried Tomato Pieces, Olive Oil, Salt, Yeast Extract, Dried Basil, Dried Parsley, Natural Flavor.

Energy Drink Mix: Purified Water, Natural Vegetable Glycerin, Polylysine (Natural Preservative).

Energy Bar: Almond Meal, Macadamia Nut Butter, Honey, Pecan, Coconut, Flaxseed Meal, Coconut Oil, Vanilla, Sea Salt.

Chip Snack: Kale, Red Bell Peppers, Cashews, Sunflower Seeds, Nutritional Yeast, Lemon Juice, Cayenne Pepper, Sea Salt.

Algal Oil: Gelatin, Glycerin, Purified Water, Turmeric (Color), Annatto Extract (Color).

Supplements

Vitamin A (as Beta Carotene), Vitamin C (Ascorbic Acid), Vitamin D (as Cholecalciferol), Vitamin E (as DL-Alpha Tocopherol Acetate), Vitamin K (as Phytonadione), Thiamine (as Thiamine Mononitrate), Riboflavin, Niacin (as Niacinamide), Vitamin B6 (as Pyridoxine HCl), Folic Acid, Vitamin B12 (as Cyanocobalamin), Biotin, Pantothenic Acid (as Calcium-D-Pantothenate), Calcium (as Calcium Carbonate and Tribasic Calcium Phosphate), Iron (as Ferrous Fumarate), Phosphorous (as Tribasic Calcium Phosphate), Iodine (as Potassium Iodine), Magnesium (as Magnesium Oxide), Zinc (Zinc Oxide), Selenium (as Sodium Selenate), Copper (as Cupric Sulfate), Manganese (as Manganese Sulfate), Chromium (as Chromium Picolinate), Molybdenum (as Sodium Molybdate). Proprietary Blend: Beet Root Powder, Spinach Leaf Powder, Tomato Fruit Powder, Carrot Root Powder, Collards Greens Powder, Collards (Kale) Leaf Powder. Other Ingredients: Stearic Acid, Microcrystalline Cellulose, Dicalcium Phosphate, Croscarmellose Sodium, Magnesium Stearate, Silicon Dioxide, Food-grade Shellac.

QUANTIFICATION AND STATISTICAL ANALYSIS

The software used for statistical analysis was GraphPad Prism v.7. The figure legends describe the statistical tests used, value of n for each experimental group, and what n represents for each experiment. All statistical analyses were two-sided and p values < 0.05 were considered significant (*$p < 0.05$, **$p < 0.01$, ***$p < 0.001$, ****$p < 0.0001$). Differences between the means of two groups were tested with Student's t test comparison, and one-way or two-way ANOVA followed by Bonferroni post-test among multiple groups. Unless otherwise specified in figure legends, all data are expressed as the mean ± SEM. All samples represent biological replicates. No samples or animals were excluded from analysis, and sample size estimates were not used. Animals were randomly assigned to experimental groups.

ADDITIONAL RESOURCES

Clinical trial registry (NCT02158897) for the human FMD trial data described in the manuscript can be found here (description: https://clinicaltrials.gov/ct2/show/study/NCT02158897?id=NCT02158897&rank=1).